

AD-A151 696

INVESTIGATION OF POTENTIAL AND VISCOUS FLOW EFFECTS
CONTRIBUTING TO DYNAMIC STALL(U) AIR FORCE INST OF TECH
WRIGHT-PATTERSON AFB OH SCHOOL OF ENGI... A J ALLAIRE
SEP 84 AFIT/GAE/AA/84S-1

1/1

UNCLASSIFIED

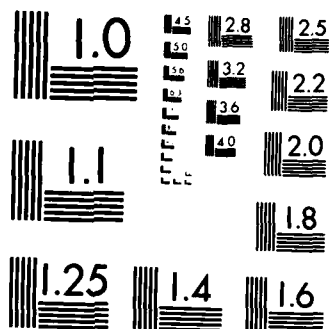
F/G 28/4

NL

END

FILED

DTIC



MICROCOPY RESOLUTION TEST CHART
NATIONAL BUREAU OF STANDARDS-1963-A

①

AD-A151 696



INVESTIGATION OF POTENTIAL
AND VISCOUS FLOW EFFECTS
CONTRIBUTING TO DYNAMIC STALL
THESIS

André J.S. Allaire
Major, CAF



DISTRIBUTION STATEMENT A

Approved for public release
Distribution Unlimited

DTIC
ELECTE
MAR 28 1985

S D

B

DEPARTMENT OF THE AIR FORCE
AIR UNIVERSITY

AIR FORCE INSTITUTE OF TECHNOLOGY

Wright-Patterson Air Force Base, Ohio

85 03 13 091

DTIC FILE COPY

AFIT/GAE/AA/84S-1

INVESTIGATION OF POTENTIAL
AND VISCOUS FLOW EFFECTS
CONTRIBUTING TO DYNAMIC STALL

THESIS

André J.S. Allaire
Major, CAF

DTIC
ELECTE
MAR 28 1985
B

AFIT/GAE/AA/84S-1

INVESTIGATION OF POTENTIAL AND VISCOUS FLOW
EFFECTS CONTRIBUTING TO DYNAMIC STALL

THESIS

Presented to the Faculty of the School of Engineering
of the Air Force Institute of Technology
Air University
In Partial Fulfillment of the
Requirements for the Degree of
Master of Science in Aeronautical Engineering

André J.S. Allaire, B.Sc.

Major, CAF

September 1984

Approved for public release; distribution unlimited

Acknowledgments

The research reported here is a continuation of the works of Major J. Lawrence and Captain K. Tupper reported in their theses. They have set the frame work of this study and greatly facilitated my task. Many of the concepts used herein originated in their work.

I am grateful for the constant aid and guidance provided by my thesis advisor, Major E. Jumper. He not only proposed the problem to me but has provided invaluable support and engineering insight throughout the investigation. Special thanks are also due to Dr. J. Hitchcock for his expert guidance during my work. Finally, I would like to thank my wife, Carole, and my children for their enduring patience and constant support over the last year.

André J.S. Allaire

Approved For	
1	<input checked="checked" type="checkbox"/>
2	<input type="checkbox"/>
3	<input type="checkbox"/>
4	<input type="checkbox"/>
5	<input type="checkbox"/>
6	<input type="checkbox"/>
7	<input type="checkbox"/>
8	<input type="checkbox"/>
9	<input type="checkbox"/>
10	<input type="checkbox"/>
11	<input type="checkbox"/>
12	<input type="checkbox"/>
13	<input type="checkbox"/>
14	<input type="checkbox"/>
15	<input type="checkbox"/>
16	<input type="checkbox"/>
17	<input type="checkbox"/>
18	<input type="checkbox"/>
19	<input type="checkbox"/>
20	<input type="checkbox"/>
21	<input type="checkbox"/>
22	<input type="checkbox"/>
23	<input type="checkbox"/>
24	<input type="checkbox"/>
25	<input type="checkbox"/>
26	<input type="checkbox"/>
27	<input type="checkbox"/>
28	<input type="checkbox"/>
29	<input type="checkbox"/>
30	<input type="checkbox"/>
31	<input type="checkbox"/>
32	<input type="checkbox"/>
33	<input type="checkbox"/>
34	<input type="checkbox"/>
35	<input type="checkbox"/>
36	<input type="checkbox"/>
37	<input type="checkbox"/>
38	<input type="checkbox"/>
39	<input type="checkbox"/>
40	<input type="checkbox"/>
41	<input type="checkbox"/>
42	<input type="checkbox"/>
43	<input type="checkbox"/>
44	<input type="checkbox"/>
45	<input type="checkbox"/>
46	<input type="checkbox"/>
47	<input type="checkbox"/>
48	<input type="checkbox"/>
49	<input type="checkbox"/>
50	<input type="checkbox"/>
51	<input type="checkbox"/>
52	<input type="checkbox"/>
53	<input type="checkbox"/>
54	<input type="checkbox"/>
55	<input type="checkbox"/>
56	<input type="checkbox"/>
57	<input type="checkbox"/>
58	<input type="checkbox"/>
59	<input type="checkbox"/>
60	<input type="checkbox"/>
61	<input type="checkbox"/>
62	<input type="checkbox"/>
63	<input type="checkbox"/>
64	<input type="checkbox"/>
65	<input type="checkbox"/>
66	<input type="checkbox"/>
67	<input type="checkbox"/>
68	<input type="checkbox"/>
69	<input type="checkbox"/>
70	<input type="checkbox"/>
71	<input type="checkbox"/>
72	<input type="checkbox"/>
73	<input type="checkbox"/>
74	<input type="checkbox"/>
75	<input type="checkbox"/>
76	<input type="checkbox"/>
77	<input type="checkbox"/>
78	<input type="checkbox"/>
79	<input type="checkbox"/>
80	<input type="checkbox"/>
81	<input type="checkbox"/>
82	<input type="checkbox"/>
83	<input type="checkbox"/>
84	<input type="checkbox"/>
85	<input type="checkbox"/>
86	<input type="checkbox"/>
87	<input type="checkbox"/>
88	<input type="checkbox"/>
89	<input type="checkbox"/>
90	<input type="checkbox"/>
91	<input type="checkbox"/>
92	<input type="checkbox"/>
93	<input type="checkbox"/>
94	<input type="checkbox"/>
95	<input type="checkbox"/>
96	<input type="checkbox"/>
97	<input type="checkbox"/>
98	<input type="checkbox"/>
99	<input type="checkbox"/>
100	<input type="checkbox"/>

A-1



Table of Contents

	Page
Acknowledgments	ii
List of Figures	iv
List of Symbols	v
Abstract	x
I. Introduction	1
Discussion	1
Problem Statement	2
Background	2
II. Theory Development	6
Introduction	6
Non-Inertial Control Volume	6
Development of the von Karman- Pohlhausen Method	18
Inviscid Solution	24
Conformal Mapping - Joukowski Transformation	30
Numerical Solution Process	33
III. Results	36
Preliminaries	36
Camber Effects	38
Thickness Effects	42
Location of Rotation Point	44
IV. Conclusion and Recommendations	46
Conclusion	46
Recommendations	47
Bibliography	49
Appendix A	51
Appendix B	53
Appendix C	57
Appendix D	64
Vita	74

List of Figures

<u>Figure</u>		<u>Page</u>
1	Results of Experimental Investigation of Dynamic Stall by Kramer, Deekens/Kuebler, Daley and Lawrence	4
2	General Non-Inertial Control Volume	8
3	Dynamics of a Pitching Airfoil	9
4	Momentum Conservation in a Non-Inertial Boundary-Layer Control Volume	14
5	Continuity in a Non-Inertial Boundary-Layer Control Volume	14
6	Hiemenz Flow	17
7	Rigid Body Rotation	24
8	Circle Theorem	28
9	Transformation Planes	32
10	Increase of Quarter-Chord Separation Angle of Attack With Camber Ratio	38
11	Joukowski Cambered Airfoil Profile	39
12	Induced Camber Model Results	41
13	Increase of Quarter-Chord Separation Angle of Attack With Thickness	43
14	Increase of Quarter-Chord Separation Angle of Attack With Location of Rotation Point	45
B1	Unsteady Separation Criteria	55
C1	Camber on a Flat Plate	57
C2	Local Angle of Attack on Rotating Flat Plate	58
C3	Local Angle of Attack on Cambered Plate	58
C4	Thick Airfoil	61

List of Symbols

a	radius of mapping circle
c	airfoil chord
c.c.w.	counter clockwise
curl	curl vector operator
dA	infinitesimal surface element
$d\bar{A}$	outward normal vector of magnitude dA
ds	infinitesimal arc length element
$dvol$	infinitesimal volume element
f	camber ratio
$f(x)$	camber function
$f_1(K)$	function of shape parameter (see equation (50))
$f_2(K)$	function of shape parameter (see equation (51))
$f_3(K)$	function of shape parameter (see equation (57))
$f_1f_2f_3$	non-inertial reference frame with origin at the rotation point
$\hat{f}_1\hat{f}_2\hat{f}_3$	unit vector along axis of $f_1f_2f_3$ reference frame
g	gravitational acceleration
h	height above airfoil surface always larger than the local boundary layer thickness, but otherwise indefinite.
k	an integration constant
\dot{m}_{TOP}	mass flow rate across the top of the control volume
r	radial position in polar coordinate

\bar{r}	position vector from the origin of the xyz non-inertial reference frame to a point in the control volume
u	x-component of V_{xyz}
v	y-component of V_{xyz}
xyz	non-inertial reference frame fixed to the airfoil surface
$\hat{x}, \hat{y}, \hat{z}$	unit vector along the axis of the xyz reference frame
w	complex velocity
\bar{A}	a general vector
AFIT	Air Force Institute of Technology
\bar{B}	body force (per unit volume)
B.L.	boundary layer
C	mass injection constant
CAF	Canadian Armed Forces
C_ℓ	lift coefficient
c.s.	control surface
c.v.	control volume
D/DT	substantive derivative
Eu_l	as defined in equation (36)
F	complex potential
$F(K)$	as defined in equation (52)
I	value of integral in equation (28)
K	shape parameter (see equation (47))
MRS	Moore-Root-Sears

P	pressure
\bar{P}	position vector from origin of inertial reference frame to a point in the control volume
\bar{R}	position vector from origin of inertial reference frame to origin of xyz non-inertial reference frame
\bar{T}	surface force (per unit area)
\bar{V}	velocity vector
V_∞	free stream velocity
XYZ	inertial reference frame
$\hat{x}, \hat{y}, \hat{z}$	unit vector along axis of XYZ reference frame
Z	as defined in equation (47)
Z plane	the airfoil plane
α	angle of attack
$\dot{\alpha}_{ND}$	non-dimensional pitch parameter
β	angle between line $\theta = 0$ from center of mapping circle and line connecting center with x-axis crossing of circle
δ	boundary-layer thickness
δ_1	boundary-layer displacement thickness
δ_2	boundary-layer momentum thickness
η	non-dimensional height above airfoil surface (y/δ)
θ	angular position in polar coordinate, or argument of a complex number, or angle between chord and R
μ	absolute viscosity, or location of center of mapping circle in Argand plane

ν	kinematic viscosity
π	the constant 3.14159265...
ρ	density, or magnitude of a complex vector
ρ plane	plane of the mapping circle with center at origin
ρ' plane	plane of the mapping circle with center off origin
τ	shear stress
ϕ	angle between tangent to airfoil surface and \bar{R} , or potential function
ψ	angle between tangent to airfoil surface and \hat{x} , or stream function
$\bar{\omega}$	angular velocity of non-inertial reference frame with respect to inertial reference frame
Γ	circulation strength
Λ	shape parameter (see equation (39))
∇	divergence operator

Subscripts

e	at the edge of the boundary-layer
$f_1 f_2 f_3$	non-inertial reference frame with origin at rotation point
$L.E.$	at the leading edge
l_0	for zero lift
0	at stagnation point
r	at rotation point, or radial component in polar coordinates

s	at stall
ss	under steady-state conditions
t	at the point where the mapping circle crosses the positive x-axis
T.E.	at the trailing edge
W or WALL	at the surface of the airfoil
xyz	non-inertial reference frame with origin on the airfoil surface
XYZ	inertial reference frame
θ	tangential component in polar coordinates
Γ_i	induced by the i^{th} shedded vortex
∞	free stream conditions

Superscripts

xyz/XYZ	from non-inertial to inertial reference frame
\wedge	unit vector
\cdot	time rate of change
$''$	second derivative with respect to time
$*$	viewed from inertial reference frame
$_$	vector

Abstract

This study explores the problem of dynamic stall, i.e. the stall of an airfoil undergoing pitching motion. The general equations of continuity and momentum are developed for a non-inertial and unsteady control volume. They are written in momentum-integral form and the boundary layer on the pitching airfoil is computed using a modified von Karman-Pohlhausen method.

The boundary layer edge velocity, velocity gradient and time rate of change of velocities required for the step by step integration of the von Karman-Pohlhausen working equations are obtained from the inviscid solution. The inviscid velocity profile along the surface of the airfoil is obtained by conformal mapping from the velocity profile around a rotating circular cylinder. Complex potential flow theory is used to obtain the velocity around the cylinder. The Kutta condition is continuously maintained at the point mapping to the trailing edge of the airfoil for each time step. This way, the flow is considered steady at each time step, but varies from one time step to the next when the angle of attack is increased. The increase in stall angle of attack is analyzed as a function of a non-dimensional pitch rate ($0.5c\dot{\alpha}/U_{\infty}$). Although the solution is obtained primarily for a symmetric Joukowski airfoil of thickness ratio 0.15 (J015), the analysis also includes variations of camber, thickness and location of the point of rotation.

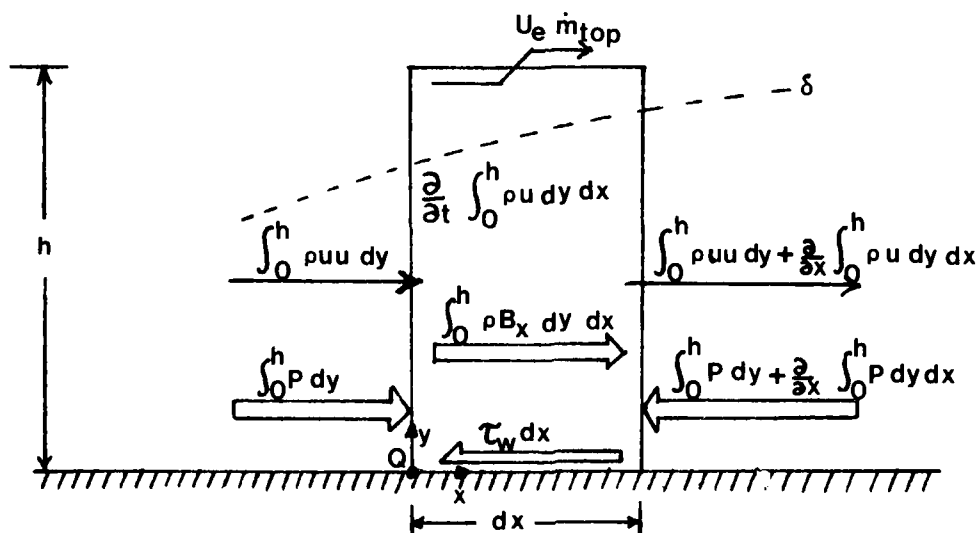


Figure 4. Momentum Conservation in a Non-Inertial Boundary-Layer Control Volume

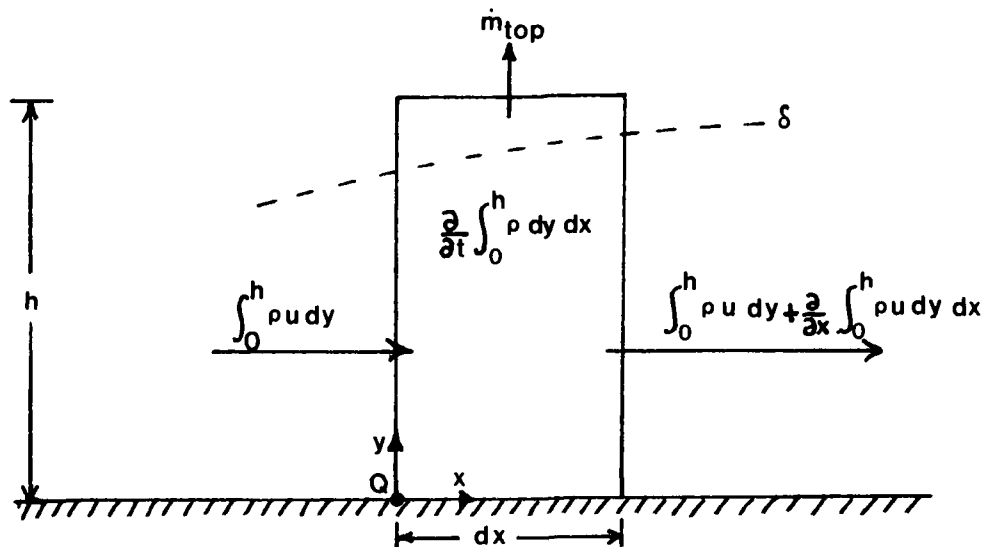


Figure 5. Continuity in a Non-Inertial Boundary-Layer Control Volume

for the general unsteady, non-inertial control volume fixed on the surface of our pitching airfoil.

Figure 4 is an expanded view of this control volume showing all the x-components of the forces acting on and within it. The control volume is of unit depth, infinitesimally narrow (dx) and of height h such that its upper side is always above the edge of the boundary layer.

Applying (20) to the c.v. of Figure 3, we get the x-component of the momentum equation for our c.v.:

$$\begin{aligned}
 & - \frac{\partial}{\partial x} \int_0^h P dy dx - \tau_w dx - \int_0^h \{ R(\ddot{\alpha} \sin \phi + \dot{\alpha}^2 \cos \phi) + 2\dot{\alpha} \dot{v} + \ddot{\alpha} y \\
 & - \dot{\alpha}^2 x \} \rho dy dx = \frac{\partial}{\partial x} \int_0^h \rho u dy + U_e \dot{m}_{TOP} + \frac{\partial}{\partial t} \int_0^h \rho u dy dx
 \end{aligned} \quad (21)$$

Now, applying the continuity equation (1) to the same control volume and assuming incompressible flow ($\rho = \text{constant}$), we get from Figure 5:

$$\dot{m}_{TOP} = - \frac{\partial}{\partial x} \int_0^h \rho u dy dx \quad (22)$$

Using (22) in (21) yields:

$$\begin{aligned}
 & - \frac{\partial}{\partial x} \int_0^h P dy dx - \tau_w dx - \int_0^h \{ R(\ddot{\alpha} \sin \phi + \dot{\alpha}^2 \cos \phi) + 2\dot{\alpha} \dot{v} + \ddot{\alpha} y - \dot{\alpha}^2 x \} \rho dy dx \\
 & = \frac{\partial}{\partial x} \int_0^h \rho u dy dx - U_e \frac{\partial}{\partial x} \int_0^h \rho u dy dx + \frac{\partial}{\partial t} \int_0^h \rho u dy dx
 \end{aligned} \quad (23)$$

We assume that our airfoil is perfectly rigid so that the quantities R, θ, ϕ, ψ are all constant while it is rotating. Then carrying out the differentiation in (12) using (13) and (11) we get:

$$\bar{V}_{XYZ} = \bar{V}_{xyz} + \dot{\alpha} [(R \sin \phi + y)\hat{x} + (R \cos \phi - x)\hat{y}] \quad (14)$$

From (14) we can compute V_{xyz} (the non-inertial velocity) from V_{XYZ} (the inertial velocity) and the dynamics of the airfoil. In the above derivation we could also have obtained:

$$\bar{R}_{XYZ} = \frac{d\bar{R}}{dt_{XYZ}} = R \dot{\alpha} (\sin \phi \hat{x} + \cos \phi \hat{y}) \quad (15)$$

Then:

$$\ddot{\bar{R}}_{XYZ} = R [(\ddot{\alpha} \sin \phi + \dot{\alpha}^2 \cos \phi) \hat{x} + (\ddot{\alpha} \cos \phi - \dot{\alpha}^2 \sin \phi) \hat{y}] \quad (16)$$

Also:

$$2 \bar{\omega} \times \bar{V}_{xyz} = 2 \dot{\alpha} (\dot{y} \hat{x} - \dot{x} \hat{y}) = 2 \dot{\alpha} (v \hat{x} - u \hat{y}) \quad (17)$$

$$\dot{\bar{\omega}} \times \bar{r} = -\ddot{\alpha} \hat{z} \times (x \hat{x} + y \hat{y}) = \ddot{\alpha} (y \hat{x} - x \hat{y}) \quad (18)$$

$$\bar{\omega} \times (\bar{\omega} \times \bar{r}) = -\dot{\alpha}^2 \hat{z} \times (x \hat{x} + y \hat{y}) \quad (19)$$

Substituting (16) thru (19) in (2), we get:

$$\begin{aligned} \oint_{c.s.} \bar{T} dA + \iiint_{c.v.} \bar{b} \rho dvol &= \iiint_{c.v.} \{ R (\ddot{\alpha} \sin \phi + \dot{\alpha}^2 \cos \phi) + 2 \dot{\alpha} v + \ddot{\alpha} y \\ &\quad - \dot{\alpha}^2 x \} \hat{x} + \{ R (\ddot{\alpha} \cos \phi - \dot{\alpha}^2 \sin \phi) - 2 \dot{\alpha} u - \ddot{\alpha} x - \dot{\alpha}^2 y \} \hat{y} \} \rho dvol \\ &= \oint_{c.s.} \bar{V}_{xyz} (\rho \bar{V}_{xyz} \cdot d\bar{A}) + \frac{\partial}{\partial t_{xyz}} \iiint_{c.v.} \bar{V}_{xyz} (\rho dvol) \end{aligned} \quad (20)$$

Its velocity is then, by definition:

$$\bar{V}_{XYZ} \equiv \frac{dP}{dt_{XYZ}} \quad (7)$$

where the time rate of change is that seen from the inertial reference frame (XYZ). Then:

$$\bar{V}_{XYZ} = \frac{d\bar{P}}{dt_{XYZ}} = \frac{d}{dt_{XYZ}} (\bar{R} + \bar{r}) = \frac{d\bar{R}}{dt_{XYZ}} + \frac{d\bar{r}}{dt_{XYZ}} \quad (8)$$

But we can write, from figure 3:

$$\bar{R} = -R \cos \phi \hat{x} + R \sin \phi \hat{y} \quad (9)$$

$$\bar{r} = x \hat{x} + y \hat{y} \quad (10)$$

$$\omega^{xyz/XYZ} = -\dot{\phi} \hat{z} \quad (\text{positive c.c.w.}) \quad (11)$$

Substituting (9) and (10) into (8):

$$\begin{aligned} V_{XYZ} &= \frac{d}{dt_{XYZ}} [-R \cos \phi \hat{x} + R \sin \phi \hat{y} + x \hat{x} + y \hat{y}] \\ &= \frac{d}{dt_{XYZ}} [(-R \cos \phi + x) \hat{x} + (R \sin \phi + y) \hat{y}] \end{aligned} \quad (12)$$

As the quantity in bracket is not expressed in the same reference frame as that in which the time derivative is taken, we need to use the general rule for the derivative of a vector:

$$\frac{d}{dt_{XYZ}} \bar{A}_{xyz} = \frac{d}{dt_{xyz}} \bar{A}_{xyz} + \bar{\omega}^{xyz/XYZ} \times \bar{A}_{xyz} \quad (13)$$

- $\hat{f}_1\hat{f}_2$: reference frame is a non-inertial reference frame with its origin at the rotation point and rotating with the airfoil.
- $\hat{x}\hat{y}$: reference frame is a non-inertial reference frame with its origin fixed at a point on the surface of the airfoil and its x-axis tangent to the surface while the y-axis is perpendicular to the surface.

The transformations between the different reference frames are:

$$\begin{aligned}\hat{X} &= (\cos\alpha) \hat{f}_1 + (\sin\alpha) \hat{f}_2 \\ \hat{Y} &= (-\sin\alpha) \hat{f}_1 + (\cos\alpha) \hat{f}_2\end{aligned}\tag{3}$$

and:

$$\begin{aligned}\hat{f}_1 &= (\cos\psi)\hat{x} + (\sin\psi)\hat{y} \\ \hat{f}_2 &= (\sin\psi)\hat{x} + (\cos\psi)\hat{y}\end{aligned}\tag{4}$$

Substituting (4) into (3) and using the trigonometric identities $\cos(\alpha - \psi) = \cos\alpha \cos\psi + \sin\alpha \sin\psi$ and $\sin(\alpha - \psi) = \sin\alpha \cos\psi - \cos\alpha \sin\psi$ will give:

$$\begin{aligned}\hat{X} &= [\cos(\alpha - \psi)]\hat{x} + [\sin(\alpha - \psi)]\hat{y} \\ \hat{Y} &= [-\sin(\alpha - \psi)]\hat{x} + [\cos(\alpha - \psi)]\hat{y} \\ \hat{Z} &= \hat{z}\end{aligned}\tag{5}$$

Consider point P in figure 3. Its position vector with respect to point O is:

$$\bar{P} = \bar{R} + \bar{r}\tag{6}$$

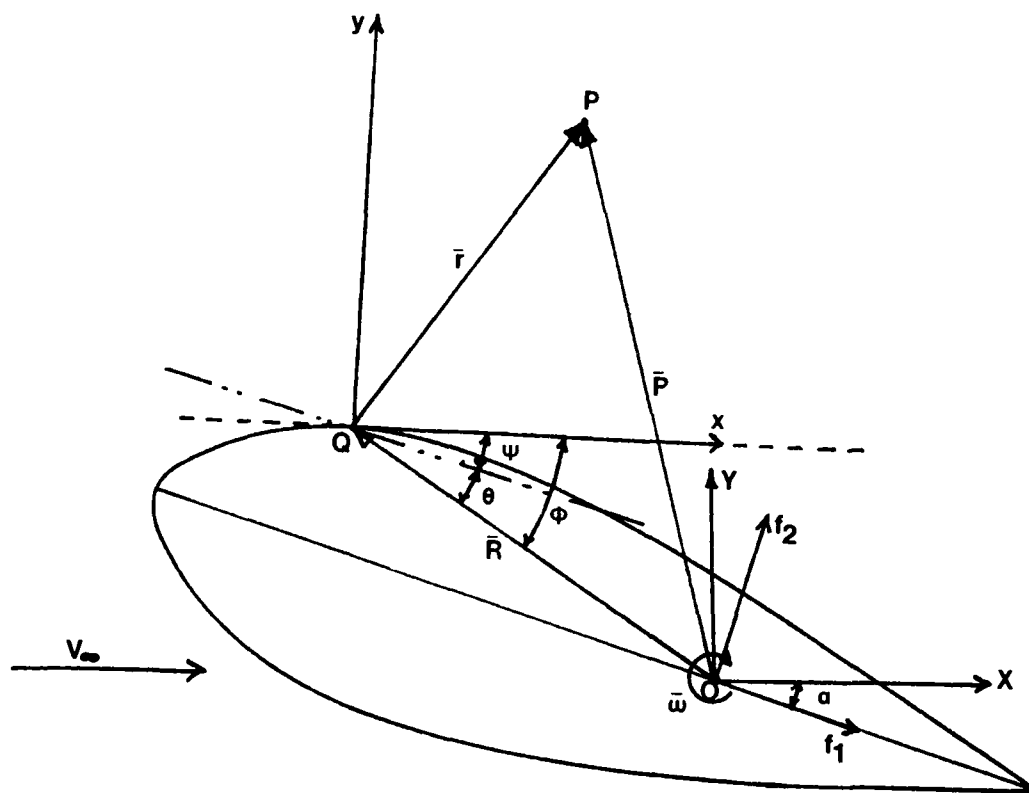


Figure 3. Dynamics of a Pitching Airfoil

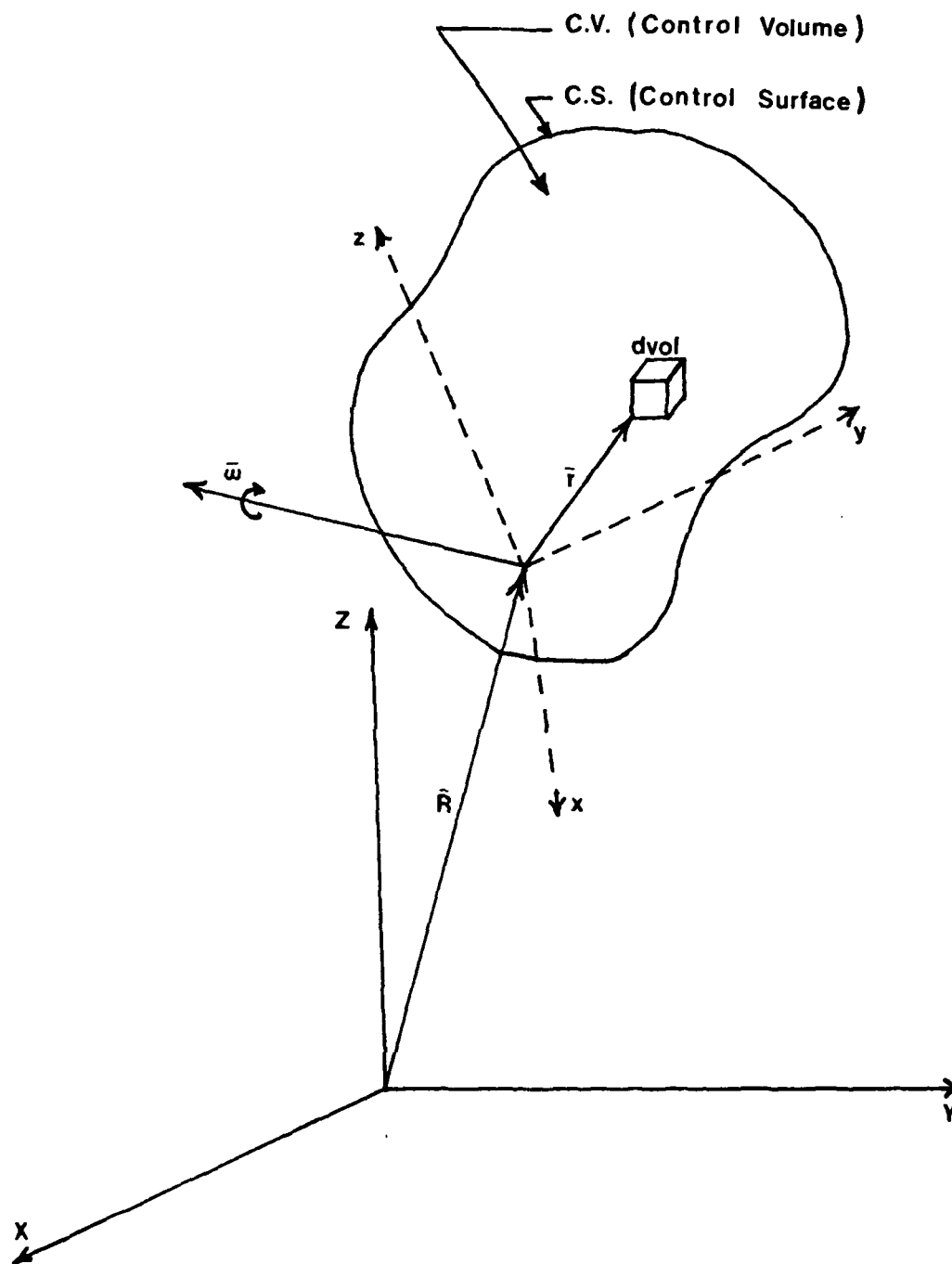


Figure 2. General Non-Inertial Control Volume

In these two basic equations, the different quantities have the following meaning (refer to figure 2):

\bar{T}	: surface forces
$d\bar{A}$: an outward normal vector to the surface element of magnitude dA
\bar{B}	: body forces in <u>an inertial c.v.</u>
\bar{V}_{xyz}	: velocity vector <u>as measured from the non-inertial c.v.</u>
$\partial/\partial t_{xyz}$: time rate of change <u>as measured from the non-inertial c.v.</u>
dA	: a surface element of the control surface
\bar{R}	: position vector from the origin of the <u>inertial reference frame</u> to the origin of the <u>non-inertial one</u>
$\bar{\omega}$: the angular velocity of the <u>non-inertial reference frame</u> with respect to the <u>inertial reference frame</u>
\bar{r}	: position vector from the origin of the <u>non-inertial reference frame</u> to the point under consideration in <u>the non-inertial reference frame</u>

We will now apply equations (1) and (2) to a specific control volume attached to an airfoil pitching in a steady air stream. We now refer to figure 3.

On figure 3 we note that:

$\hat{X}\hat{Y}$: reference frame is the inertial reference frame with its origin at the rotation point.

II. Theory Development

Introduction

The flow about a pitching airfoil is solved analytically using a von Karman-Pohlhausen momentum integral technique. Because our control volume is attached to the airfoil, the basic equation for continuity and momentum must first be derived for a non-inertial control volume. Finally, the velocity at the edge of the boundary layer is obtained from the inviscid solution.

Non-Inertial Control Volume

We wish to develop the continuity and momentum equations for a control volume attached to the surface of an airfoil undergoing a pitching motion in a steady stream.

For the most general control volume, the continuity equation is given by (7:141-145):

$$\oint_{c.s.} \rho \bar{V}_{xyz} \cdot d\bar{A} = -\frac{\partial}{\partial t_{xyz}} \iiint_{c.v.} \rho \, dvol \quad (1)$$

and the linear momentum equation by:

$$\begin{aligned} & \oint_{c.s.} \bar{r} dA + \iiint_{c.v.} \bar{B} \rho \, dvol - \iiint_{c.v.} [\bar{R} + 2\bar{\omega} \times \bar{V}_{xyz} + 2\dot{\bar{\omega}} \times \bar{r} + \bar{\omega} \times (\bar{\omega} \times \bar{r})] \rho \, dvol \\ &= \oint_{c.s.} \bar{V}_{xyz} (\rho \bar{V}_{xyz} d\bar{A}) + \frac{\partial}{\partial t_{xyz}} \iiint_{c.v.} \bar{V}_{xyz} (\rho \, dvol) \end{aligned} \quad (2)$$

he investigated the pitching airfoil problem and empirically derived rules for predicting the effect of a constant pitch rate on the lift of airfoils of different thicknesses and camber ratios.

In this study, the viscous flow analysis developed by Lawrence is used; however, the potential flow solution makes use of a new concept originating from a jump condition observed by Tupper. The rotational motion of the airfoil is modeled by an induced camber. Although a closer match to the experimental results is desirable, the thrust of this study is toward achieving better physical insight into the problem rather than a perfect match of the experimental results. To this end, some assumptions are made to alleviate the mathematical difficulties or complexities which could obscure the problem.

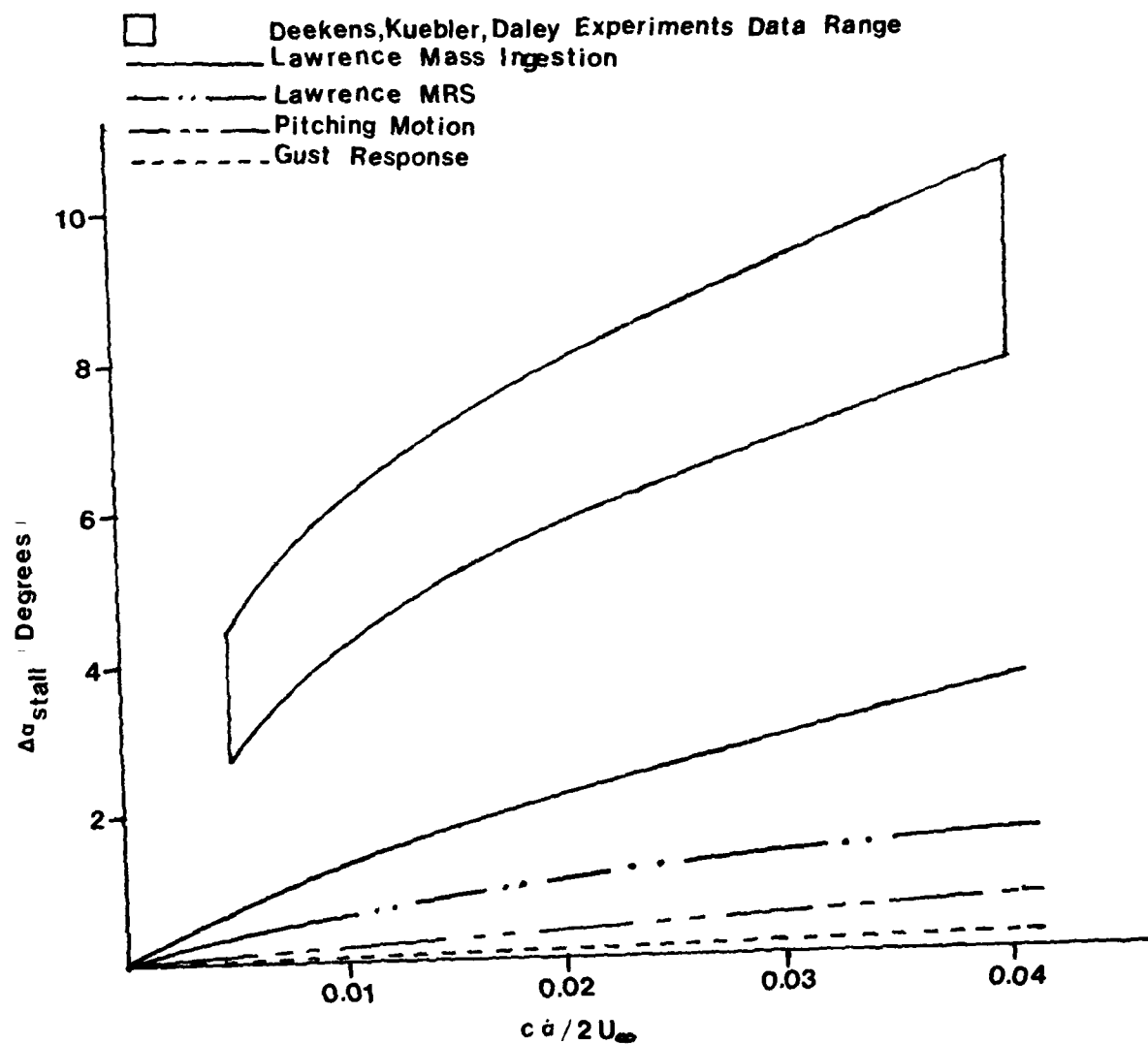


Figure 1. Results of Experimental Investigation of Dynamic Stall by Kramer, Deekens/Kuebler, Daley and Lawrence

(1). In his experimental set-up, the airfoil was fixed in the wind tunnel between a set of movable guide vanes; he used those vanes to make a constant change of the angle of attack on the airfoil.

In 1978, Deekens and Kuebler (2) and in 1982, Daley (3) conducted experimental studies on a pitching airfoil in a constant velocity smoke tunnel. Their results are combined in figure 1. There is a considerable difference between the gust experiment and the pitching airfoil one. Docken (4) has related the increase in the stall angle of attack of the gust problem to a reduction of the adverse pressure gradient imposed on the boundary-layer.

In 1983, Lawrence (5) investigated in detail the pitching airfoil problem using a von Karman-Pohlhausen momentum-integral technique and related some of the increase in the stall angle of attack to the same reduction of the adverse pressure gradient; further portions of the gain were related to a change in flow separation criterion due to the moving boundary (Moore-Root-Sears models) and, mostly, mass introduction into the boundary-layer from the external flow. His results are also included in figure 1.

During the same year, Tupper (6) made an analytical study of the potential flow about an airfoil starting from rest. He modeled the unsteadiness of the flow by using vortex shedding at the trailing edge. Using the same method,

the stall occurs at a significantly greater angle of attack and is much more severe than in the case when the stall angle of attack is very slowly approached (i.e. static stall conditions). The contributing factors to this phenomenon are both viscous and inviscid; they depend on pitch rate, free-stream velocity, airfoil geometry, Reynolds number and Mach number (10:304).

Problem Statement

The purpose of this thesis is to improve the knowledge of the physical contributors to the phenomenon of dynamic stall. A modified von Karman-Pohlhausen momentum-integral method is used to analyze the flow within the boundary layer, while a complex potential flow theory is used to analyze the inviscid flow. Conformal mapping is used to obtain the flow around the airfoil from that of a circular cylinder. By using these relatively simple techniques, it is easier to keep track of the underlying physics of the problem.

This study is restricted to the analysis of a pitching airfoil in a steady flow field; as the control volume used to study the boundary layer is attached to this pitching airfoil, non-newtonian fluid mechanics is used.

Background

In 1932, Max Kramer published the results of his experimental study of a dynamic stall induced by a wind gust

INVESTIGATION OF POTENTIAL AND VISCOUS FLOW EFFECTS CONTRIBUTING TO DYNAMIC STALL

I. Introduction

Discussion

The phenomenon of dynamic stall has received considerable attention from fluid dynamicists since 1930. However, most of the research has been experimental and the results empirical. Unsteady aerodynamics has been developed mainly for small amplitude oscillatory displacements about an equilibrium position. Dynamic stall is obviously important to the helicopter and the compressor industries; here again, however, the amplitude of the movements about an equilibrium angle of attack is small enough to allow the use of perturbation theory. Consequently, there is still much to be learned about the dynamic stall problem.

In this study, we analyze the behavior of the unsteady flow pattern about an airfoil that is pitched from steady prestall conditions until dynamic stall is reached. The total angle of attack excursion may be as large as 40 to 50 degrees, making any use of perturbation theories impossible. When the airfoil is stalled under such a dynamic condition,

Dividing thru by ρdx , we get:

$$\begin{aligned}
 & -\frac{1}{\rho} \int_0^h \frac{\partial P}{\partial x} dy - \frac{\tau_w}{\rho} - \int_0^h \{ R(\ddot{\alpha} \sin \phi + \dot{\alpha}^2 \cos \phi) + 2\dot{\alpha} \dot{v} + \ddot{\alpha} y - \dot{\alpha}^2 x \} dy \\
 & = \int_0^h \frac{\partial}{\partial x} (uu) dy - u_e \int_0^h \frac{\partial u}{\partial x} dy + \int_0^h \frac{\partial u}{\partial t} dy
 \end{aligned} \tag{24}$$

where the order of integration and differentiation has been interchanged. We note that in (24) all time derivatives and velocities are those measured from the non-inertial reference frame (\hat{x}, \hat{y}) .

At this point, we need to derive the non-inertial Euler equation to solve for $\partial P / \partial x$. In Appendix A, we show that this equation, when applied to the streamline at the edge of the boundary layer, is given by:

$$-\frac{1}{\rho} \frac{\partial P}{\partial x} = u_e \frac{\partial u_e}{\partial x} + \frac{\partial u_e}{\partial t} + \{ R(\ddot{\alpha} \sin \phi + \dot{\alpha}^2 \cos \phi) + 2\dot{\alpha} \dot{v}_e + \ddot{\alpha} \delta - \dot{\alpha}^2 x \} \tag{25}$$

Substituting (25) into (24) and grouping terms, we get:

$$\begin{aligned}
 & \frac{\tau_w}{\rho} - \int_0^h \left[u_e \frac{\partial u_e}{\partial x} + \frac{\partial}{\partial t} (u_e - u) + 2\dot{\alpha} (\dot{v}_e - v) + \ddot{\alpha} (\delta - y) \right] dy \\
 & = - \int_0^h \frac{\partial}{\partial x} (uu) dy + u_e \int_0^h \frac{\partial u}{\partial x} dy
 \end{aligned} \tag{26}$$

It can easily be shown that (5:64-65)

$$- \int_0^h \frac{\partial}{\partial x} (uu) dy + u_e \int_0^h \frac{\partial u}{\partial x} dy = \frac{\partial}{\partial x} (u_e^2 \delta_2) + u_e \left(\frac{\partial u_e}{\partial x} \right) \delta_1$$

and
$$\int_0^h \frac{\partial}{\partial t} (u_e - u) dy = \frac{\partial}{\partial t} (u_e \delta_1)$$

where δ_1 and δ_2 are the displacement and momentum thickness, respectively.

Therefore (26) can be written as:

$$\frac{\tau_w}{\rho} = \frac{\partial}{\partial x} (u_e^2 \delta_2) + u_e \left(\frac{\partial u_e}{\partial x} \right) \delta_1 + \frac{\partial}{\partial t} (u_e \delta_1) + \int_0^h [2\dot{\alpha}(v_e - v) + \ddot{\alpha}(\delta - y)] dy \quad (27)$$

In the derivation of (27), the only assumptions made were:

- a) rigid airfoil;
- b) incompressible flow;
- c) center of rotation located on airfoil chord;
- d) two dimensional flow;
- e) $\partial P / \partial x = dP / dx$; and;
- f) Weight of fluid in c.v. negligible.

Before proceeding to transform (27) into the von Karman-Pohlhausen working equation, we analyze its last term:

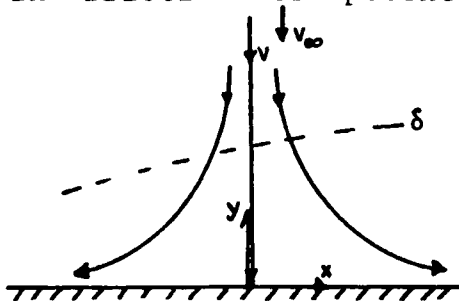
$$I = \int_0^h \{2\dot{\alpha}(v_e - v) + \ddot{\alpha}(\delta - y)\} dy \quad (28)$$

The second term of I gives:

$$\int_0^h \ddot{\alpha}(\delta - y) dy = \ddot{\alpha} \left(\delta h - \frac{h^2}{2} \right) \quad (29)$$

There remains to integrate the first term. As a first approximation, we can treat the y-component of the velocity as a Hiemenz flow (stagnation flow in plane) for which an

exact solution exists (8:95-99). The velocity distribution in frictionless potential flow in the vicinity of the stagnation point is given by:



$$\begin{aligned} u &= a x v_{\infty} \\ v &= -a y v_{\infty} \end{aligned} \quad (30)$$

Figure 6. Hiemenz Flow

Now

$$\int_0^h 2\dot{\alpha} (v_e - v) dy = 2\dot{\alpha} v_e \int_0^h \left(1 - \frac{v}{v_e}\right) dy$$

From (30):

$$\frac{v}{v_{\infty}} = -a y \quad \text{and} \quad \frac{v_e}{v} = -a \delta$$

Therefore
$$\frac{v}{v_e} = \frac{y}{\delta}$$

So that

$$\int_0^h 2\dot{\alpha} (v_e - v) dy = 2\dot{\alpha} v_e \left(h - \frac{h^2}{2\delta}\right) \quad (31)$$

Therefore

$$I = \ddot{\alpha} \left(\delta h - \frac{h^2}{2}\right) + 2\dot{\alpha} \left(h - \frac{h^2}{2\delta}\right) v_e$$

As I will eventually be evaluated at $y = \delta$, we pose immediately:

$$I = \ddot{\alpha} \frac{\delta^2}{2} + \dot{\alpha} \delta v_e$$

so that (27) becomes:

$$\frac{\tau_w}{\rho} \frac{\partial(u_e^2 \delta_2)}{\partial x} + u_e \frac{\partial u_e}{\partial x} \delta_1 + \frac{\partial}{\partial t} (u_e \delta_1) + \ddot{\alpha} \frac{\delta^2}{2} + \dot{\alpha} \delta v_e \quad (32)$$

Development of the Von Karman-Pohlhausen Method

In the development of the von Karman-Pohlhausen working equation, we follow the procedure described by Schlichting (8:206-223).

If we expand the derivatives in the momentum integral equation (27), multiply it by $\delta_2 / \nu u_e$ and use the closure equation (5:13-25), we get:

$$\begin{aligned} \frac{\tau_w \delta_2}{\mu u_e} = & \frac{\delta_2}{\nu} u_e \frac{\partial \delta_2}{\partial x} + \left(2 + \frac{\delta_1}{\delta_2}\right) \frac{\delta_2^2}{\nu} \frac{\partial u_e}{\partial x} + \frac{1}{2} \frac{\delta_1}{\delta_2} \frac{\delta_2^2}{\nu} \frac{1}{u_e} \frac{\partial u_e}{\partial t} \\ & + \frac{1}{\nu} \frac{\delta_2}{u_e} \end{aligned} \quad (33)$$

Adding and subtracting the quantity

$$\begin{aligned} \left(2 + \frac{1}{2} \frac{\delta_1}{\delta_2}\right) \frac{\delta_2^2}{\nu} \left(\frac{1}{u_e} \frac{\partial u_e}{\partial t}\right) + \left(2 + \frac{\delta_1}{\delta_2}\right) \frac{\delta_2^2}{\nu} \{R(\ddot{\alpha} \sin \phi + \dot{\alpha}^2 \cos \phi) \\ + 2\dot{\alpha} v_e + \ddot{\alpha} \delta\} \end{aligned} \quad (34)$$

gives

$$\begin{aligned} \left(2 + \frac{\delta_1}{\delta_2}\right) \frac{\delta_2^2}{\nu} E u_1 + u_e \frac{\delta_2}{\nu} \frac{\partial \delta_2}{\partial x} + \frac{\delta_2 I}{\nu u_e} - \left(2 + \frac{1}{2} \frac{\delta_1}{\delta_2}\right) \frac{\delta_2^2}{\nu} \left(\frac{1}{u_e} \frac{\partial u_e}{\partial t}\right) \\ = \frac{\tau_w \delta_2}{\mu u_e} \end{aligned} \quad (35)$$

where:

$$Eu1 = R(\ddot{\alpha}\sin\phi + \dot{\alpha}^2\cos\phi) + 2\dot{\alpha}v_e + \ddot{\alpha}\delta + \frac{\partial u_e}{\partial x} + \frac{1}{u_e} \frac{\partial u_e}{\partial t} \quad (36)$$

We now assume that the velocity profile within the boundary-layer has the form:

$$\frac{u}{u_e} = A + B\eta + C\eta^2 + D\eta^3 + E\eta^4 \quad (37)$$

where $\eta = y/\delta$, and is subjected to the boundary conditions:

$$\begin{aligned} \text{at } y=0 : u &= 0 & \frac{v\partial^2 u}{\partial y^2} &= -(Eu1)u_e \\ \text{at } y=\delta : u &= u_e & \frac{\partial u}{\partial y} &= 0 & \frac{\partial^2 u}{\partial y^2} &= 0 \end{aligned} \quad (38)$$

We define

$$\Lambda = \frac{\delta^2}{\nu} Eu1 \quad (39)$$

and solve (37) for its coefficient by applying the five boundary conditions; we get

$$\begin{aligned} A &= 0 \\ B &= 2 + \frac{\Lambda}{6} \\ C &= -\frac{\Lambda}{2} \\ D &= -2 + \frac{\Lambda}{2} \\ E &= 1 - \frac{\Lambda}{6} \end{aligned} \quad (40)$$

The velocity profile is then given in terms of Λ by:

$$\frac{u}{u_e} = (2\eta - 2\eta^3 + \eta^4) + \frac{\Lambda}{6} (\eta - 3\eta^2 + 3\eta^3 - \eta^4) \quad (41)$$

By applying the definition of the displacement and momentum thickness, we get (8:209)

$$\frac{\delta_1}{\delta} = \frac{3}{10} - \frac{\Lambda}{120} \quad (42)$$

$$\frac{\delta_2}{\delta} = \frac{37}{315} - \frac{\Lambda}{945} - \frac{\Lambda^2}{9072} \quad (43)$$

The shear stress at the wall is given by

$$\tau_W = \mu \frac{\partial u}{\partial y} \Big|_{y=0} \quad (44)$$

so that

$$\frac{\tau_W \delta}{\mu u_e} = 2 + \frac{\Lambda}{6} \quad (45)$$

If we assume that separation occurs when the shear stress at the wall is zero, then from (45), $\Lambda = -12$ at separation. However, Moore, Root and Sears have developed a better model for separation for the case of a moving wall (13:123-126). In Appendix B, we show that the value of Λ at separation is given by the solution of:

$$\frac{(\Lambda_S + 12)^2}{512(\Lambda_S - 6)^3} (9\Lambda^2 - 136\Lambda + 528) = - \frac{u_{WALL}}{u_e} \quad (46)$$

where u_{WALL} is the tangential component of the wall velocity at the separation point.

Let us now define:

$$Z \equiv \frac{\delta_2^2}{v} \quad (47)$$

$$K \equiv Z \text{ Eu1} \quad (48)$$

Then, from (39), (43) and (48) the shape factors K and Λ satisfy the universal relation:

$$K = \left(\frac{37}{315} - \frac{\Lambda}{945} - \frac{\Lambda^2}{9072} \right)^2 \Lambda \quad (49)$$

Let us also define

$$f_1(K) \equiv \frac{\delta_1}{\delta_2} = \left(\frac{3}{10} - \frac{\Lambda}{120} \right) \left(\frac{37}{315} - \frac{\Lambda}{945} - \frac{\Lambda^2}{9072} \right)^{-1} \quad (50)$$

$$f_2(K) \equiv \frac{\tau_w \delta_2}{\mu u_e} = \left(2 + \frac{\Lambda}{6} \right) \left(\frac{37}{315} - \frac{\Lambda}{945} - \frac{\Lambda^2}{9072} \right) \quad (51)$$

$$F(K) = 2f_2(K) - 4K - 2Kf_1(K) \quad (52)$$

and note that (from (47)):

$$u_e \frac{\delta_2}{v} \frac{\partial \delta_2}{\partial x} = \frac{1}{2} u_e \frac{dZ}{dx} \quad (53)$$

Then, if we substitute (47) thru (53) in (35) and rearrange some terms, we get:

$$\begin{aligned} \frac{dZ}{dx} = \frac{1}{u_e} \{ & F(K) + \{4 + f_1(K)\} \frac{Z}{u_e} \frac{\partial u_e}{\partial t} + R(\ddot{\alpha} \sin \phi + \dot{\alpha}^2 \cos \phi) \\ & + 2\dot{\alpha} v_e + \ddot{\alpha} \delta - \frac{2\delta_2 I}{u_e} \} \end{aligned} \quad (54)$$

$$Z = K(\text{Eu1})^{-1} \quad (55)$$

where again, Eul is given by (36). In this set of equations, the quantities $\dot{\alpha}$, $\ddot{\alpha}$, R and ϕ are known from the geometry and the dynamics of the problem; the quantities $F(K)$, $f_1(K)$, $f_2(K)$ are functions only of the shape parameter K (or Λ); finally the other quantities u_e , v_e , $\partial u_e / \partial x$, $\partial u_e / \partial t$, I and Eul are derivable from the inviscid flow outside the boundary layer. However, two problems remain to be solved. First, to evaluate I , we need to make some assumption, such as the Hiementz flow assumption of page 17. In this case:

$$\frac{2\delta_2 I}{u_e} = \frac{2}{u_e} \frac{\delta_2^2}{u} \frac{\delta}{\delta_2} \left(\frac{\ddot{\alpha}\delta + \dot{\alpha}v_e}{2} \right) = \frac{2}{u_e} Z f_3(K) \left(\frac{\ddot{\alpha}\delta + \dot{\alpha}v_e}{2} \right) \quad (56)$$

$$\text{where } f_3(K) = \frac{\delta}{\delta_2} \quad (57)$$

Second, δ occurs directly in the term $\ddot{\alpha}\delta$ of (54) and in Eul . We therefore have a closure problem as the value of δ is required not only for these terms but also to obtain the value of V_e from inviscid flow. A computer iteration routine could be used to evaluate $\delta(x)$. As we start from steady state conditions before subjecting the airfoil to a pitching motion, $\dot{\alpha} = \ddot{\alpha} = 0$ and we recover the steady, non-inertial von Karman-Pohlhausen working equations from (54) and (55). Their integration will provide the initial boundary-layer thickness distribution $\delta(x)$. As the pitching motion start, (54) and (55) are solved using the previous $\delta(x)$ and so on till separation occurs at the quarter chord. This should

yield an exact solution of the pitching airfoil dynamic stall problem within the assumptions made on pages 16 and 17. An offset of this approach would be the study of the change of the boundary-layer thickness due to the pitching motion, and the effect of this change on the dynamic stall.

An alternative approach is that of Lawrence (5). He showed that the effect of the hypothetical (non-inertial) body forces on a control volume where the upper limit is the edge of the boundary layer can be neglected. Then he used the unsteady but inertial Euler equation:

$$u_e^* \frac{\partial u_e^*}{\partial x} + \frac{\partial u_e^*}{\partial t} = \frac{1}{\rho} \frac{dP}{dx} \quad (58)$$

where U_e^* is the velocity viewed from the inertial reference frame, and assumed that

$$u_e = u_e^* - R\dot{\alpha} \sin\phi \quad (59)$$

He finally accounted for the non-inertial conditions by assuming that mass was ingested in the boundary layer through the superposition of a Hiementz flow. His development of the Von Karman-Pohlhausen method leads to the equations:

$$\frac{dZ}{dx} = \left\{ F(K) + [4 + f_1(K)] \frac{Z}{u_e} \frac{\partial u_e}{\partial t} + [4 + 2f_1(K) - 2f_3(K)] \cdot \right. \\ \left. \frac{Z R \dot{\alpha} \sin\phi}{u_e} \frac{\partial u_e}{\partial x} + 2 \left(\frac{c}{\delta} \right) z f_3(K) R \dot{\alpha} \cos\phi \right\} \frac{1}{u_e} \quad (60)$$

and

$$Z = K \left[(R \dot{\alpha} \sin\phi) \frac{1}{u_e} \frac{\partial u_e}{\partial x} + \frac{\partial u_e}{\partial x} + \frac{1}{u_e} \frac{\partial u_e}{\partial t} \right]^{-1} \quad (61)$$

For the Joukowski pitching airfoil and the Hiementz flow model, he used $C = 4 \delta$. His model achieved considerable improvement in the insight of factors contributing to the dynamic stall effects. As it has the advantage of not requiring any a priori knowledge of $\delta(x)$, it is used in the rest of this study.

Inviscid Solution

In order to solve the modified von Karman-Pohlhausen equations, we need to evaluate the velocity at the edge of the boundary-layer, U_e . In this section, we used potential flow theory and conformal mapping to evaluate it.

Figure 7 represents the flow of a circular cylinder of unit radius undergoing rigid body rotation. The vorticity is

given by:

$$\bar{\omega} = \text{curl } \bar{V} \quad (62)$$

For rigid body rotation:

$$U_r = 0 \quad U_\theta = -\dot{\alpha} r \quad (63)$$

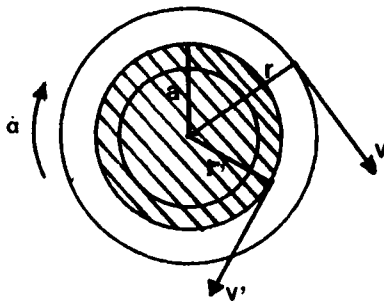


Figure 7. Rigid Body Rotation

The minus sign occurs because θ is positive counter-clockwise, therefore

$$\bar{\omega} = -2\dot{\alpha} \hat{k} \quad (64)$$

For any given time, v and v' are constant and tangent to their respective circles. Applying Stokes's circulation theorem to these two circles gives, and as $ds = r d\theta$:

$$\oint_{r'} v' ds = -2\dot{\alpha}\pi r'^2 \quad r' < a \quad (65a)$$

and

$$\oint_r v ds = -2\dot{\alpha}\pi \quad r > a \quad (66a)$$

The second integral is evaluated at $r = a = 1$ as only the cylinder is rotating and therefore the area between $r = 1$ and $r = r$ contributes nothing to the integral. Since v' and v are constant on their respective circle, we also have

$$\oint_{r'} v' ds = v' 2\pi r' \quad (65b)$$

$$\oint_r v ds = v 2\pi r \quad (66b)$$

By comparing (65) and (66) we find:

$$v' = -\dot{\alpha} r'$$

we have a rigid rotator for $r < a$; and

$$v = -\dot{\alpha} / r$$

a vortex centered at $r = 0$ and of strength $\Gamma_R = +2\pi\dot{\alpha}$ when $r > a$.

We conclude that the flow outside a rotating cylinder may be accurately modelled by superposition of the flow about

a non-rotating cylinder and the flow induced by a vortex of strength $+2\pi\dot{\alpha}$ located at the center of the circle. In order to satisfy Helmholtz's vortex Laws (17:54), we must assume that a vortex of equal and opposite strength simultaneously appears at infinity.

The stream function (ψ) and the potential function (ϕ) for the flow about a non-rotating cylinder with circulation in a free stream of uniform velocity U_∞ and having an angle of attack α are in polar coordinates (r, θ) given by (12:84):

$$\psi = r U_\infty \sin(\theta - \alpha) \left(1 - \frac{a^2}{r^2}\right) + \frac{\Gamma}{2\pi} \ln \left(\frac{r}{a}\right) \quad (67)$$

$$\phi = r U_\infty \cos(\theta - \alpha) \left(1 + \frac{a^2}{r^2}\right) - \frac{\Gamma}{2\pi} \theta \quad (68)$$

The velocities at any point (r, θ) are then

$$U_r = U_\infty \cos(\theta - \alpha) \left(1 - \frac{a^2}{r^2}\right) \quad (69)$$

$$U_\theta = -U_\infty \sin(\theta - \alpha) \left(1 + \frac{a^2}{r^2}\right) - \frac{\Gamma}{2\pi r} \quad (70)$$

On the surface of the cylinder, $r = a$ and therefore $U_r = 0$ everywhere (from (69)) and:

$$U_\theta = -2U_\infty \sin(\theta - \alpha) - \frac{\Gamma}{2\pi a}$$

We apply the Kutta condition in order to have a stagnation point at the trailing edge; i.e. for $\theta = 0$, we obtain the steady state vortex strength:

$$\Gamma_{ss} = 4\pi a U_{\infty} \sin \alpha_{ss} \quad (71)$$

We now superpose the vortex due to the rotation to the above non-rotating cylinder in steady state conditions. The stream and potential functions become, for a cylinder of unit radius:

$$\psi = r U_{\infty} \sin(\theta - \alpha) \left(1 - \frac{1}{r^2}\right) + \left(\frac{\Gamma}{2\pi} + \dot{\alpha}\right) \ln r \quad (72)$$

$$\phi = r U_{\infty} \cos(\theta - \alpha) \left(1 + \frac{1}{r^2}\right) - \left(\frac{\Gamma}{2\pi} + \dot{\alpha}\right) \theta \quad (73)$$

From (72) we find that U_r is still given by (69) and therefore remains zero everywhere on the surface. But now:

$$U_{\theta} = -U_{\infty} \sin(\theta - \alpha) \left(1 + \frac{1}{r^2}\right) - \left(\frac{\Gamma}{2\pi} + \dot{\alpha}\right) \frac{1}{r} \quad (74)$$

In this study, group together the two circulation terms so that $\frac{\Gamma'}{2\pi} = \frac{\Gamma}{2\pi} + \dot{\alpha}$, and Γ'_{ss} is still given by (71). The reason we choose to group these terms, is to obtain results which can be compared with those of Tupper.

As rotation occurs, the angle of attack is continuously changing. From (71) we see that this continuously increases Γ_{ss} ; this particular augmentation does not occur instantaneously, however. Tupper (6;5-18) has developed a procedure of vortex shedding at the trailing edge to account

for the progressive growth of the circulation following an impulsive start of angular rotation.

In this method, a vortex is shed in the wake of the airfoil behind the trailing edge. At the same time a bound vortex of equal and opposite strength is inserted inside the airfoil. The location of the shedded vortex is $U_\infty \Delta t$ where Δt is the time elapsed since the start of the impulsive motion; the bound vortex is located inside the airfoil in such a way that the surface of the airfoil remains a streamline and that the Kutta condition is maintained.

In terms of the flow about the circular cylinder, which will eventually be mapped into the airfoil, it can be shown that the Kutta condition needs to be applied at $\theta = 0$ (11:469) and that the location of the pair of vortices is obtained from the circle theorem (12:84-85). This way, referring to

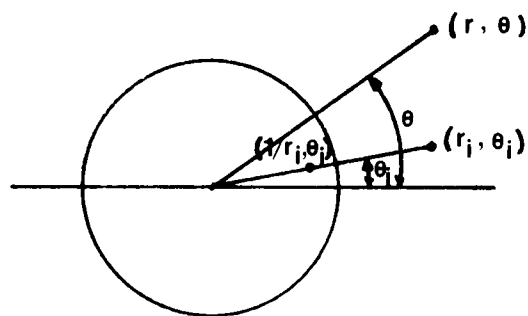


Figure 8, if the shedded vortex is located at (r_i, θ_i) , the surface remains a streamline if the bounded member of the pair is at $(1/r_i, \theta_i)$. The contribution of this pair to the stream function is then:

Figure 8. Circle Theorem

$$\psi_{\Gamma_i} = \frac{\Gamma_i}{4\pi} \ln \left[\frac{1}{r_i^2} \frac{1 + r_i^2 r^2 - 2r_i r \cos(\theta - \theta_i)}{r^2 + r_i^2 - 2r_i r \cos(\theta - \theta_i)} \right] \quad (75)$$

phenomenon, then the relaxation coefficient used in the mass ingestion model is not four but something larger. Perhaps this relaxation coefficient should be a function of position along the airfoil. Larger coefficients could be rationalized near the leading edge where relaxation distances are smaller.

In this study, the induced camber was assumed to build up instantaneously to its value specified by the non-dimensional pitch rate; however, pitch rate does take a finite time period to attain its steady-state value. This effect would certainly reduce the reported induced camber effect, although the magnitude of the reduction could only be estimated from more precise knowledge of the experimental apparatus used by Deekens and Kuebler (2).

Thickness Effect

The mass ingestion model program was run for symmetrical Joukowski airfoils of different thickness ratios, represented by the value the real part of μ in the plane transformation given by equation (82). The effect of thickness on the increase in separation angle of attack ($\Delta\alpha_{sep}$) due to the pitching motion is shown in figure 13. $\Delta\alpha_{sep}$ increases with thickness for all pitch rates.

For thin airfoils (real part of μ on the order of 0.05 or less), separation occurred at the leading edge under static conditions. The dynamic effect could therefore not be

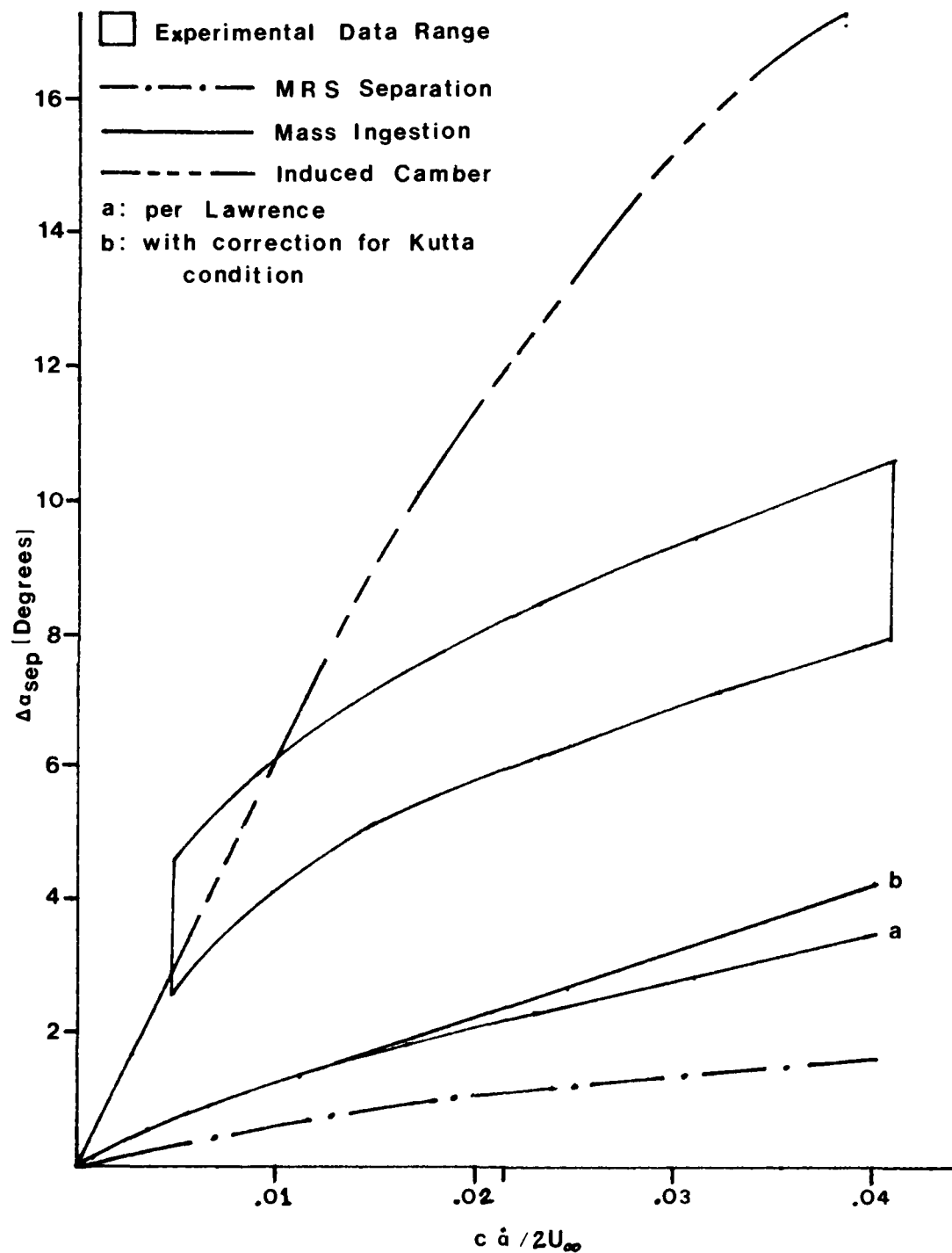


Figure 12. Induced Camber Model Results

Our induced camber model, is then applied as follows:

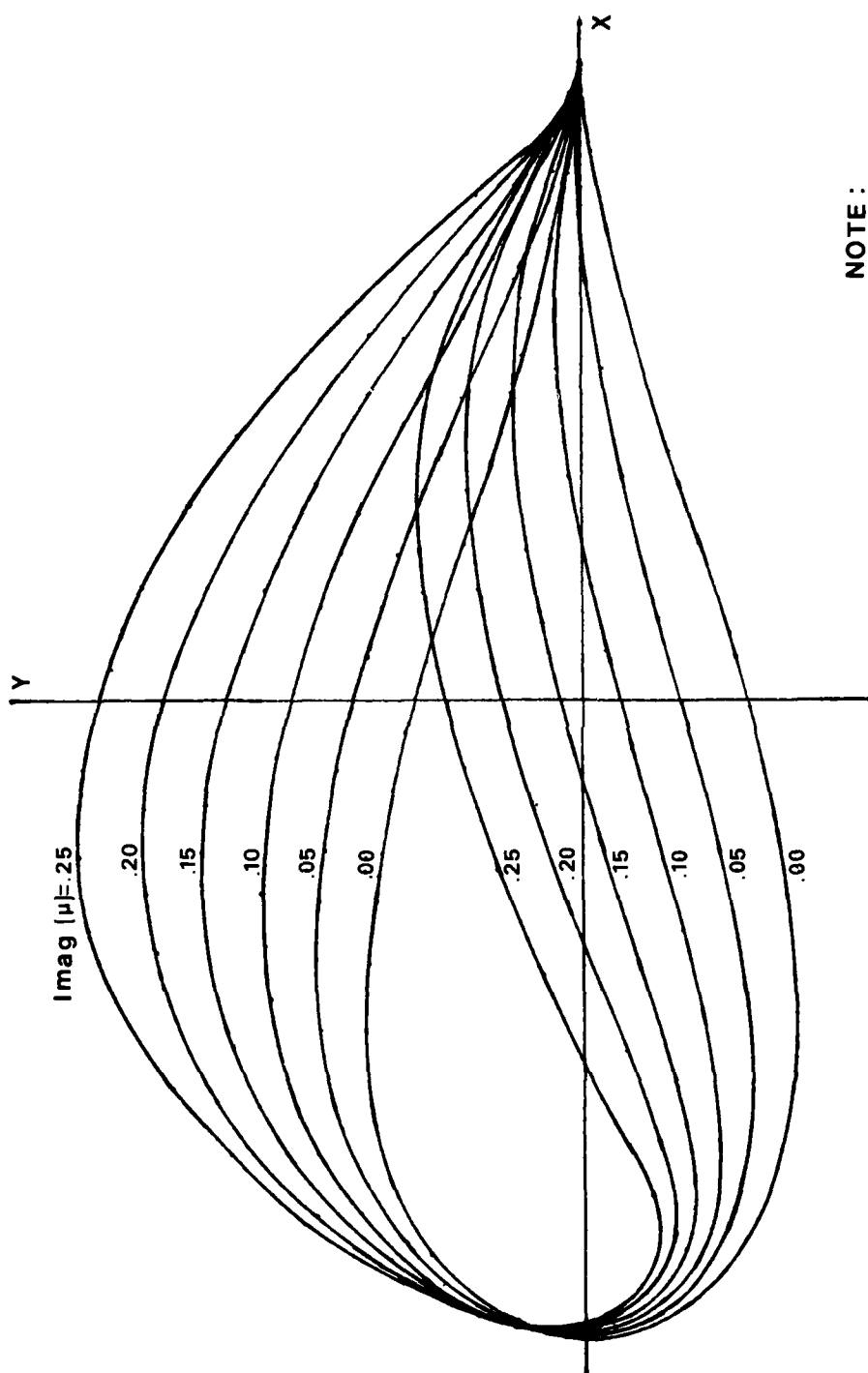
a) as the model represents the rotating motion of the airfoil, it replaces the mass ingestion model used by Lawrence (5:47-51); its effect is therefore added to the MRS line of figure 1;

b) from Appendix C, the camber induced by the rotating motion of an airfoil of type J015 is:

$$f/c = 3.47 \dot{\alpha}_{ND}$$

therefore, for any given $\dot{\alpha}_{ND}$, the increase in static stall angle of attack is obtained from the data of figure 10 and added to the MRS curve for the same $\dot{\alpha}_{ND}$.

The result is shown in figure 12. The induced camber effect is very large, much larger than expected. A review of the data compiled for laminar airfoils by Althaus (18:13-20) does not show such an increase; the fact that a Joukowski airfoil has a circular arc profile with its maximum close to the half chord, while laminar profiles has parabolic camber with maximum close to the quarter-chord could explain this discrepancy. It was anticipated that the induced camber effect would fall short of the experimental data range when superimposed on the pitch and MRS effects. If, as we think, induced camber and mass ingestion model the same physical



NOTE :
The Y scale is twice
as large as the X
scale

Figure 11. Joukowski Cambered Airfoil Profile

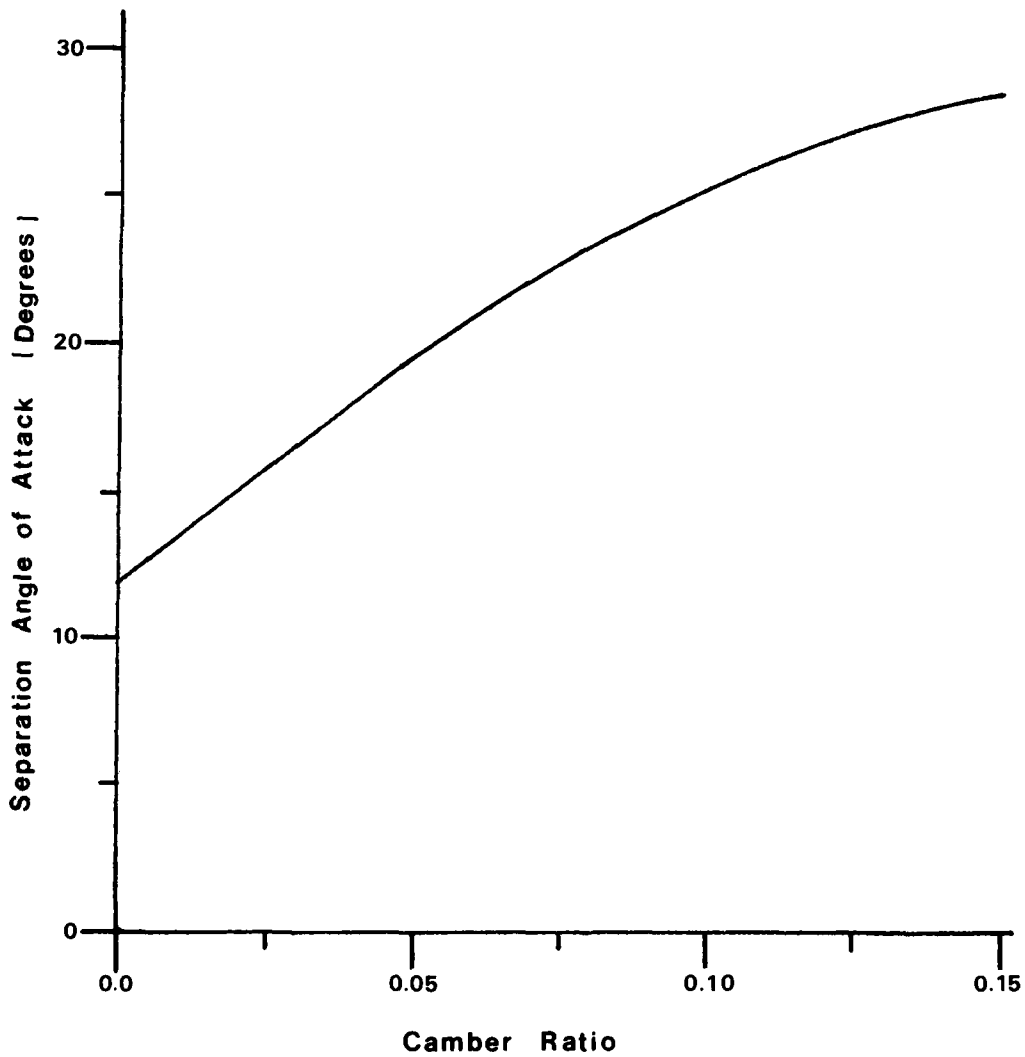


Figure 10. Increase of Quarter-Chord Separation Angle of Attack With Camber Ratio

Camber Effect

As the results of Lawrence (5:53) fall short of the experimental data, an effort was made to find other contributing factors to the dynamic stall. Tupper's results (6:56) for a rotating cylinder showed an unexplained jump in lift coefficient immediately after the start of pitching motion; as a camber airfoil has such a jump over its corresponding symmetrical airfoil, it was hypothesized that the rotating motion could be modeled by an induced camber, as shown in Appendix C.

The program was then run for airfoil of different camber ratio but having the same thickness ratio. The result was that camber had no noticeable effect on the curves $\Delta \alpha_{sep}$ versus $c\alpha/2U_\infty$ for both the MRS and mass injection cases shown in figure 1. However, the static quarter-chord separation angle of attack sharply increases with camber ratio as shown in figure 10, where the camber ratios were measured from the plots of the airfoil shown in figure 11 as a function of the vertical displacement of the mapping circle, i.e. the imaginary part of the complex number μ of the plane transformation given by equation (82).

To obtain the true static separation angle of attack for a cambered airfoil, the value of α_{sep} obtained from the program had to be reduced by the value of β used in the plane transformation given by equation (82); this difference is strictly due to the geometry of the transformation.

III. Results

Preliminaries

Before attempting to progress from the results of Lawrence and Tupper, several modifications were made on Lawrence program (5:91-96). Firstly, it was generalized to compute the boundary layer of a general Joukowski airfoil of arbitrary thickness and camber ratios; secondly, it was modified to accept any location for the point of rotation of the airfoil; thirdly, a procedure was incorporated to compute the quarter-chord separation criterion in accordance with the MRS model developed in Appendix B; and finally, a correction had to be made in the subroutine computing the velocity to properly account for the Kutta condition at the trailing edge.

The program was then run for a symmetric Joukowski airfoil of thickness ratio 0.15 at zero degree angle of attack. The results matched those published by Schlichting (8:213) for the same test conditions, providing assurance that the program was working properly.

Different combinations of thickness and camber could then be studied as a function of a non-dimensional pitch parameter ($0.5 c\alpha/2U_\infty$). It has been shown that when this parameter is used, the individual values given to c , α or U_∞ do not effect the results as long as they combine into the same parameter value.

The required values of $\partial U_e / \partial s$ and U_e were obtained from the non-inertial value of the first part and using

$$\frac{\partial U_e}{\partial s} = \frac{\Delta u}{\Delta \theta} \left[\frac{\Delta \theta}{\Delta s} \right]$$

where $\Delta \theta = 2$ and $\Delta s = ((y(\theta + .01)) - y(\theta - .01))^2 + (x(\theta + .01) - x(\theta - .01))^2)^{1/2}$.

For this part, the integration was started with the airfoil at any initial angle of attack without pitching motion to allow the flow to stabilize around the forward stagnation point. The pitching motion was then started, and the von Karman-Pohlhausen equations were integrated from the stagnation point to the quarter-chord. The MRS separation criterion developed in Appendix B was used to check for separation at the quarter-chord; if separation did not occur, the solution was repeated using a larger initial angle of attack.

of attack; this way, for a symmetrical airfoil, the steady-state circulation is zero, and steady-state conditions exist from the start. The velocity at the surface of the airfoil was computed from equations (70) and (71) for any required angular position in the plane. $\partial u / \partial \theta$ was also computed using finite differences as $\partial u / \partial \theta = (U(\theta + .01) - U(\theta - .01)) / \Delta \theta$, where $\Delta \theta = .02$. For this first step, $\partial u / \partial t$ is zero everywhere on the surface, i.e. steady-state condition. The airfoil was then continuously pitched by increments $\Delta \alpha = \dot{\alpha} \Delta t = 0.01$ degrees. For each α , the velocity U , and the velocity gradient $\partial u / \partial \theta$ were computed as for the case of $\alpha = 0$. The local time rate of change of velocity was also computed by finite differences as

$$\frac{\partial u}{\partial t} = \frac{u(\alpha + \Delta \alpha) - u(\alpha - \Delta \alpha)}{2 \Delta t}$$

where $\Delta t = \Delta \alpha / \dot{\alpha}$. A subroutine was then used to compute the non-inertial velocity (using equation (14)) from the above inertial velocity.

For the second part, the von Karman-Pohlhausen working equations (59) and (60) were numerically integrated using the isoclines method. The initial conditions required are (8:211):

$$\begin{aligned} K_0 &= 0.0770 \\ Z_0 &= 0.0770 / (u/x)_0 \\ (dz/dx)_0 &= -0.0652 (2U/x^2)_0 / (u/x)^2 \end{aligned}$$

The velocity in the Z plane will be

$$w(z) = \frac{dF}{dz} = \frac{dF}{d\rho} \frac{d\rho}{d\rho'} \frac{d\rho'}{dz} \quad (86)$$

but from (82)

$$\frac{d\rho'}{d\rho} = e^{-i\beta} \quad (87)$$

which has a magnitude equal to 1; and from (83)

$$\frac{dz}{d\rho'} = 1 - \left(\frac{\rho t'}{\rho'} \right)^2 \quad (88)$$

The velocity distribution in the Z plane is obtained by substituting (87) and (88) into (86), to get:

$$w(z) = e^{+i\beta} \left[1 - \left(\frac{\rho t'}{\rho'} \right)^2 \right]^{-1} w(\rho) \quad (89)$$

where $w(\rho) = u(\rho) - i v(\rho)$ is known from equation (77) and (78). As we are only interested in the velocity on the surface of the airfoil in the Z plane, only the magnitude of $w(z)$ is required; its direction must be tangent to the surface everywhere.

We now have all the elements required to solve the pitching airfoil problem.

Numerical Solution Process

The numerical solution to the pitching airfoil problem was done in two parts. First the velocity distribution at the surface of the airfoil was obtained. We started with the non rotating airfoil sitting in a steady flow at zero angle

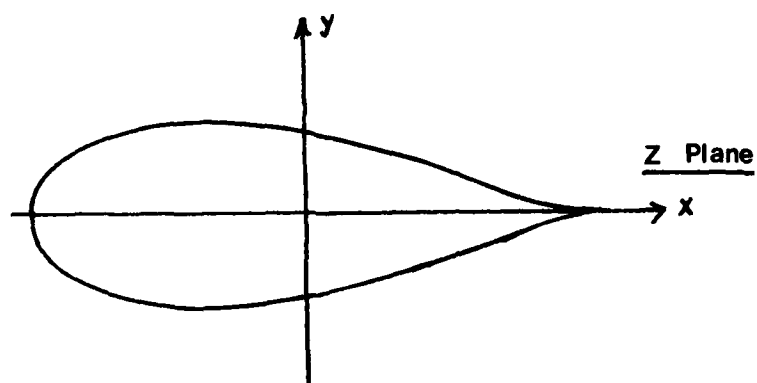
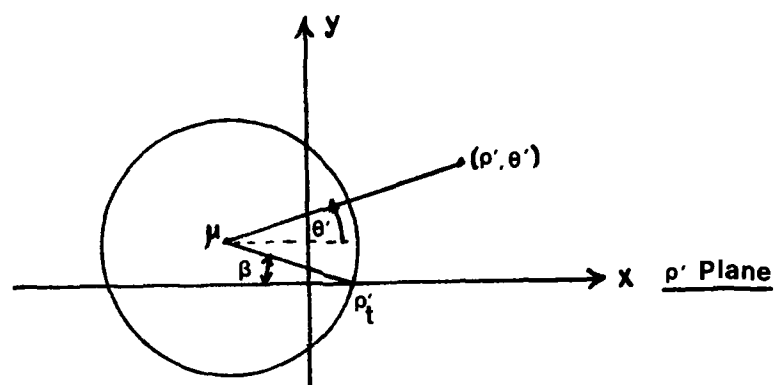
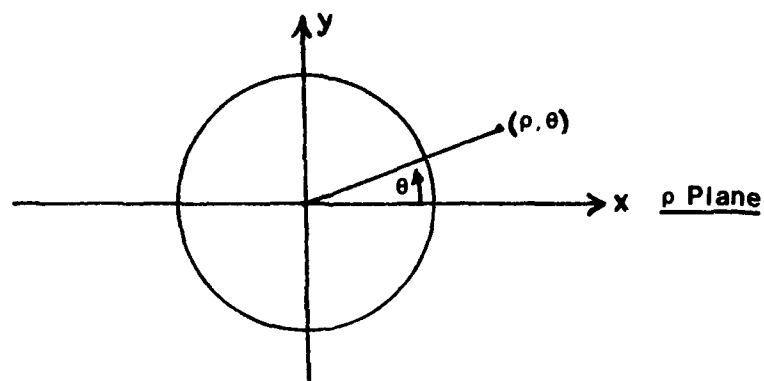


Figure 9. Transformation Planes

center is at the origin of the ρ plane. If a point in this plane is given by $\rho = r e^{i\theta}$, then it can be transformed to a ρ' plane by (11:461)

$$\rho' = \rho e^{-i\beta} + \mu \quad (82)$$

The ρ' plane has all the points of the ρ plane rotated β radians clockwise and displaced a distance μ . It therefore represents the flow about a rotating cylinder with its center located at μ , a complex number. The flow may now be transformed to that about a Joukowski airfoil (the Z plane) by the transformation.

$$Z = \rho' + \frac{\rho_t'^2}{\rho'} \quad (83)$$

The point ρ_t' is that point of the ρ' plane where the cylinder circumference crosses the positive x -axis; it maps to the trailing edge of the Joukowski airfoil.

Knowing the velocity distribution in the ρ plane and the mapping functions from the ρ to the ρ' and on to the Z plane, we can find the velocity distribution in the Z plane. If ϕ and ψ are the potential and stream functions associated with the flow in the ρ plane, we can form the complex potential

$$F(\rho) = \phi + i\psi \quad (84)$$

where $\rho = x + iy$, in the ρ plane; the complex velocity in the ρ plane is then:

$$w(\rho) = \frac{dF}{d\rho} \quad (85)$$

For the first pair, $N = 1$ and on the surface $r = 1$; then applying the Kutta condition for $\theta = 0$ and solving for Γ_1 , we get:

$$\Gamma_1 = 4\pi U_\infty \sin(\alpha - \sin \alpha_{ss}) \frac{(r_1 - 1)}{r_1^2 (r_1 + 1)} \quad (79)$$

this shedded vortex is located at

$$\begin{aligned} r_1 &= 1 + U_\infty \Delta t \\ \theta_1 &= 0 \end{aligned} \quad (80)$$

The k^{th} vortex pairs are evaluated similarly once the first $K-1$ pairs are known. In general,

$$\Gamma_k = \frac{1}{r_k^2} \left(\frac{r_k - 1}{r_k + 1} \right) 4\pi U_\infty (\sin \alpha - \sin \alpha_{ss}) - \sum_{i=1}^{k-1} \Gamma_i r_i^2 \left(\frac{r_i^2 - 1}{1 + r_i^2 - 2r_i \cos \theta_i} \right) \quad (81)$$

Again (r_k, θ_k) is given by (80) while the position of the previously shed vortices is given by:

$$r_i = r_{i,t-\Delta t} + U_r \Delta t$$

$$\theta_i = \theta_{i,t-\Delta t} + U_\theta \Delta t$$

where U_r and U_θ are computed from (77) and (78) and indicates position before the time increment.

Conformal Mapping - Joukowski Transformation

Equations (77) and (78) give us the velocity at any point of the flow field about a rotating cylinder whose

After a second time increment Δt , a second vortex is shed at $U_\infty \Delta t$, while the first vortex has moved in the flow by a distance $U \Delta t$, where U is the velocity of the flow at the original vortex location (r_1, θ_1) . And so on with each time increment. At each step, Γ can be computed by applying the Kutta condition at $\theta = 0$.

The complete model for the stream function of our rotating cylinder, where the rotation starts instantaneously from steady-state conditions of U_∞ and $\alpha = \alpha_{ss}$, is then:

$$\psi = r U_\infty \sin(\theta - \alpha) \left(1 - \frac{1}{r^2}\right) + 2 U_\infty \sin \alpha_{ss} \ln r + \sum_{i=1}^N \psi_{\Gamma_i} \quad (76)$$

where the ψ_{Γ_i} are given by (75). As time passes, the strength of the vortices remains constant, but their location changes in accordance with the flow velocity at their prior location in the field. The strength of the first pair is evaluated from the Kutta condition. Then the strength of the following pair may be computed as that of all previous pairs is known.

From (75) and (76), we get:

$$U_r = \frac{1}{r} \frac{\partial \psi}{\partial \theta} = U_\infty \cos(\theta - \alpha) \left(1 - \frac{1}{r^2}\right) \quad (77)$$

so that for $r = 1$, $U_r = 0$ and the surface is a streamline as required. Also:

$$u_\theta = -\frac{\partial \psi}{\partial r} = -U_\infty \sin(\theta - \alpha) \left(1 + \frac{1}{r^2}\right) - \frac{2 U_\infty \sin \alpha_{ss}}{r^2} - \sum_{i=1}^N \frac{\Gamma_i r_i^2}{2\pi} \left[\frac{r_i^2 r - r_i \cos(\theta - \theta_i)}{1 + r^2 r_i^2 - 2 r r_i \cos(\theta - \theta_i)} - \frac{r - r_i \cos(\theta - \theta_i)}{r^2 + r_i^2 - 2 r r_i \cos(\theta - \theta_i)} \right] \quad (78)$$

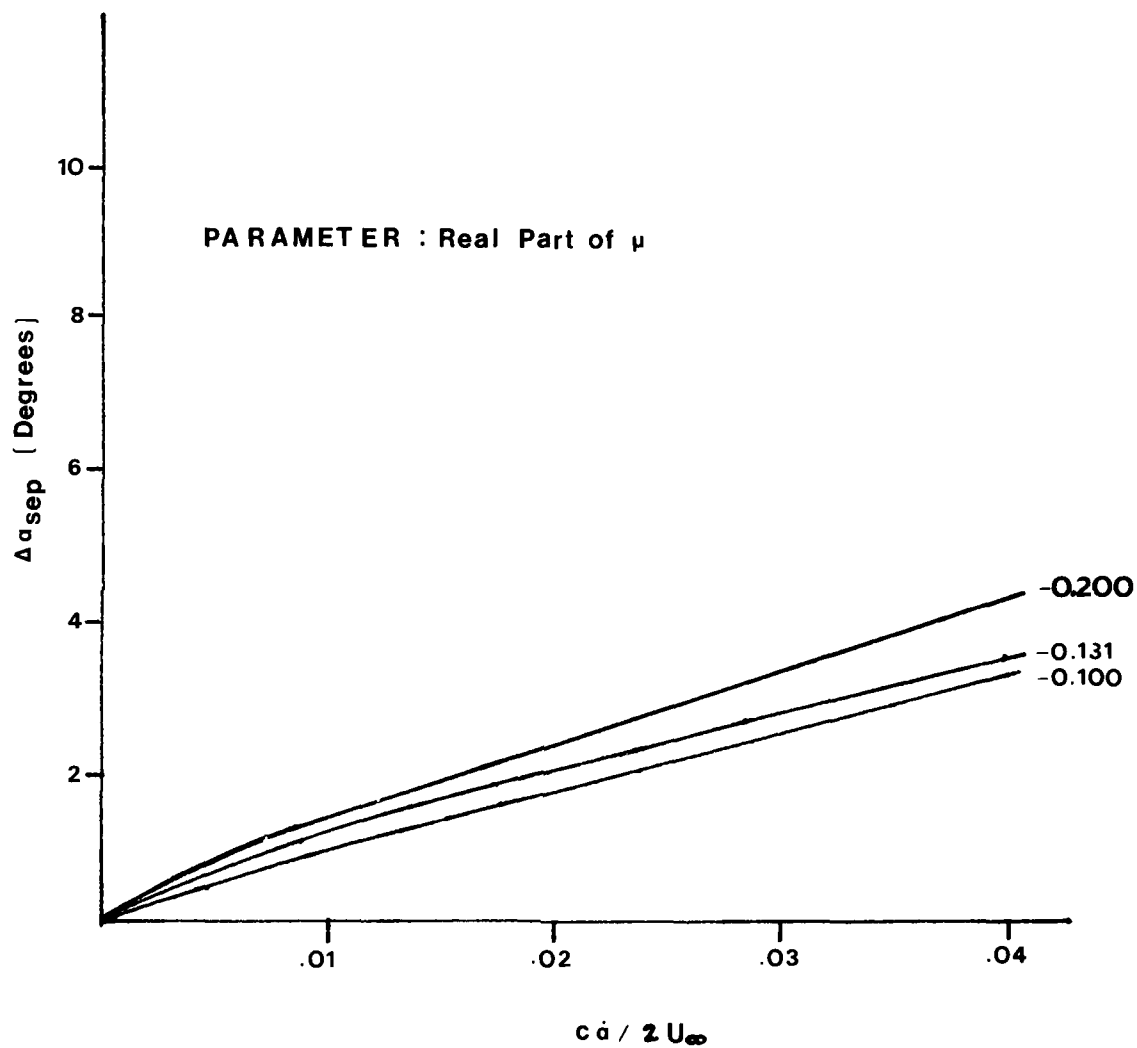


Figure 13. Increase of Quarter-Chord Separation Angle of Attack With Thickness

studied. This result is compatible with the well known leading edge bubble separation (9:220).

Location of the Point of Rotation

Another factor which could affect the results, is the location about which the airfoil undergoes its pitching motion. As the point of rotation is moved toward the trailing edge, the stream velocity induced by the pitching motion is increased, for the same value of $\dot{\alpha}_{ND}$ when compared to rotation about the mid-chord point. It was therefore expected that, on one side, more mass would be ingested at corresponding points on upper surface of the airfoil ahead of the rotation point and, on the other side, the MRS contribution would be increased as the wall velocity increases. Both effects would tend to increase the quarter-chord separation angle.

The program was run for several locations of the rotation point and the results, shown in figure 14, confirmed our expectations.

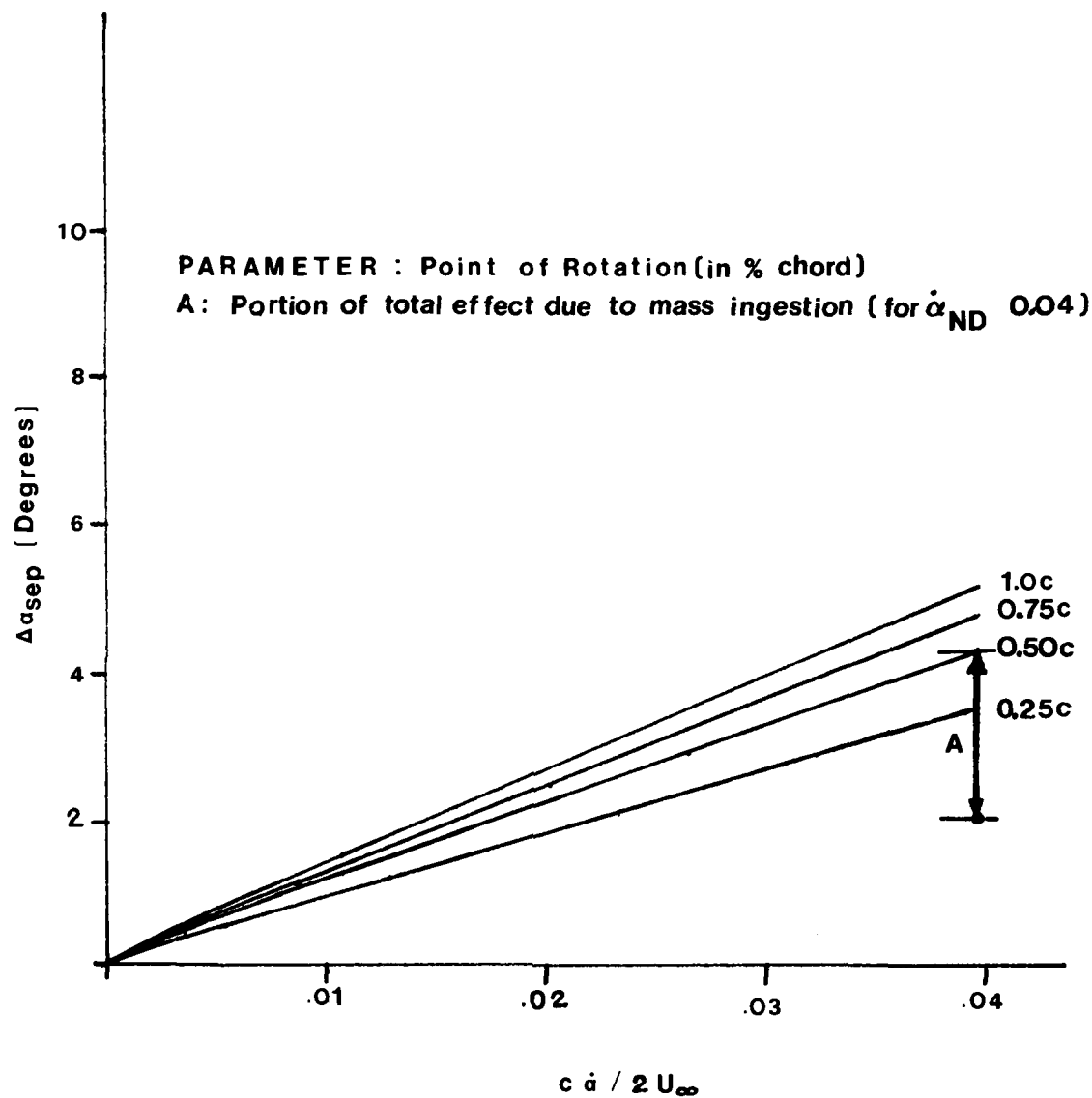


Figure 14. Increase of Quarter-Chord Separation Angle of Attack With Location of Rotation Point

IV. Conclusion and Recommendations

Conclusion

It has been shown that as an airfoil pitches at a constant $\dot{\alpha}$, the separation angle of attack is significantly increased. This increment is more pronounced for thicker airfoils; as the point of rotation moves from the leading to the trailing edge of the airfoil, $\Delta\alpha_{sep}$ also increases.

Camber was shown to have no significant effect on the viscous solution, i.e. the value of $\Delta\alpha_{sep}$ when computed as the difference between the dynamic and static separation angles of attack for the same cambered airfoil. However, a very large increase in static stall angle of attack, when compared to that of the same thickness but uncambered airfoil, was obtained.

An effort was made to model the pitching motion of a symmetrical airfoil by an induced camber due to rotation. The results obtained show a substantial increase in $\Delta\alpha_{sep}$. While the mass ingestion model results are below the experimental results, the induced camber model gives larger results. If the hypothesis of induced camber is correct, then some other factors contributing to the dynamic quarter-chord separation must therefore exist, to reduce the camber effect to the experimental data range. Camber build-up time delay could be such a factor. Separation aft of the quarter-chord would also change the pressure distribution over the

airfoil; in this study, such aft separation effects have been neglected but this too might partially explain differences.

Recommendations

This study has raised many unanswered questions; it is recommended that the following be further studied:

- a) A computer program which would use the velocity distribution about a circular cylinder shedding discrete vortices at its point mapping to the trailing edge, as developed by Tupper, would be more representative of the gradual build-up of circulation about the airfoil, and should be combined with the momentum-integral method to produce a better airfoil pitching model.
- b) Equations (54) and (55) resulted from making fewer assumptions than those used in the actual computer program. A procedure on how to use them is given on page 22; the computer program should be updated accordingly. As explained previously, this method should be more accurate: not only were fewer assumptions made, in its development, but the closure equation (5:13) is not required for its solution. It could also be used for the study of the time rate of change of the boundary-layer thickness due to pitching motion.

Further work needs to be done to resolve the question of whether mass ingestion and induced camber model the same physical phenomenon. If they do, then the relaxation coefficient used in Lawrence mass ingestion model is not four but something larger. Perhaps this relaxation coefficient should be a function of position along the airfoil (i.e., larger coefficients could be rationalized near the leading edge where relaxation distances are smaller).

Bibliography

1. Kramer, Von M. "Die Zunahme des Maximalauftriebes von Tragflugen bei plotzlicher AnstellwinkervergroBerung (Boeneffekt)", Zeitschrift fur Flugtechnik und Motorluftschiffahrt, 7:185-189
2. Deekens, A.C. and W.R. Kuebler, Jr. "A Smoke Tunnel Investigation of Dynamic Separation", Aerodynamics Digest, Fall 1978. USAFA - TR - 79 - 1, Air Force Academy, CO., Feb. 1979.
3. Daley, D.C. The Experimental Investigation of Dynamic Stall Thesis, AFIT/GAE/AA/82D-6. Air Force Institute of Technology, Wright-Patterson AFB, OH, 1983.
4. Docken, R.G., Jr. "Gust Response Prediction of an Airfoil Using a Modified von Karman-Pohlhausen Technique". Thesis, AFIT/GAE/AA/82D-9, Air Force Institute of Technology, Wright-Patterson AFB, OH, 1982.
5. Lawrence, Maj. J.S. Investigation of Effects Contributing to Dynamic Stall Using a Momentum - Integral Method. Thesis, AFIT/GAE/AA/83D-12. Air Force Institute of Technology, Wright-Patterson AFB, OH, 1983.
6. Tupper, Capt K.W. The Effect of Trailing Vortices on the Production of Lift on an Airfoil Undergoing a Constant Rate of Change of Angle of Attack. Thesis, AFIT/GAE/AA/83D-24. Air Force Institute of Technology, Wright-Patterson AFB, OH, 1983.
7. Shames, H.I. Mechanics of Fluids (Second Edition). New York: McGraw-Hill Book Company, 1982.
8. Schlichting H. Boundary Layer Theory (Seventh Edition). New York: McGraw-Hill Book Company, 1979.
9. Schlichting H. and Truckenbrodt E. Aerodynamics of the Airplane (Second Edition). New York: McGraw-Hill Book Company, 1979.
10. McCroskey, W.J. "Unsteady Airfoils", Annual Review of Fluid Mechanics, 14:285-311 (1982).
11. Karamchett, Krishnamurty. Principle of Ideal - Fluid Aerodynamics. New York: John Wiley and Sons, Inc., 1966.

12. Milne - Thompson, L.M. Theoretical Aerodynamics (Third Edition). London: MacMillan and Company Limited, 1958.
13. Williams, James C. III. "Incompressible Boundary-Layer Separation", Annual Review of Fluid Mechanics, 9:113-144 (1977).
14. Beyer, William H. CRC Standard Mathematical Tables. (26th Edition). Boca Raton, Florida: CRD Press, Inc., 1981.
15. Jumper, Eric J. "Examining a Rule of Thumb for the Relation between Camber and Zero - Lift Angle of Attack". Aeronautics Digest: 21-40 (Fall/Winter 1980).
16. Hoerner, Sighard F. and Borst, Henry V. Fluid Dynamic Lift. Brick Town, N.J.: Hoerner (1975).
17. Kuethe, Arnold M. and Chow, Chuen-Yen. Foundations of Aerodynamics: Bases of Aerodynamic Design. (Third Edition). New York: John Wiley and Sons, 1976.
18. Althaus, Dieter. Profilpoharew Fur Den Modellflug. Karlaruhe, Germany: Neckar-Verlag, 1980.

Appendix A

Derivation of the Unsteady, Non-Inertial Euler Equation

For a non-inertial reference frame, Shames shows (7:141-144) that:

$$d\bar{F} - dm [\ddot{\bar{R}} + 2\bar{\omega} \times \bar{V}_{xyz} + \bar{\omega} \times \bar{r} + \bar{\omega} \times (\bar{\omega} \times \bar{r})] = \frac{D}{Dt_{xyz}} (dm \bar{V}_{xyz}) \quad (A.1)$$

For the case where pressure P is the only surface force (i.e. no viscous force) and the weight of the fluid in the c.v. is the only body force, we have

$$d\bar{F} = -g(\nabla Z) \rho \, dvol - \nabla p \, dvol \quad (A.2)$$

If we substitute (A.2) in (A.1) and divide thru by $\rho dvol = dm$, we get:

$$\begin{aligned} -\frac{1}{\rho} \nabla p - g \nabla Z - [\ddot{\bar{R}} + 2\bar{\omega} \times \bar{V}_{xyz} + \bar{\omega} \times \bar{r} + \bar{\omega} \times (\bar{\omega} \times \bar{r})] \\ = \frac{D}{Dt_{xyz}} \bar{V}_{xyz} = (\bar{V}_{xyz} \cdot \nabla) \bar{V}_{xyz} + \frac{\partial \bar{V}_{xyz}}{\partial t_{xyz}} \end{aligned} \quad (A.3)$$

This is the general non-inertial, unsteady Euler equation. We now apply (A.3) at the edge of the boundary layer, in the c.v. shown in Figure 3 of the main text.

We take only the x-component of (A.3) and neglect gravity forces, (note here that even if we had not neglected these in both the momentum equation and Euler equation, they would cancel out) we get:

$$-\frac{1}{\rho} \frac{\partial P}{\partial x} - \left\{ \ddot{\bar{R}} + 2\bar{\omega} \times \bar{V}_{xyz} + \bar{\omega} \times \bar{r} + \bar{\omega} \times (\bar{\omega} \times \bar{r}) \right\} \Big|_x = u \frac{\partial u}{\partial x} + v \frac{\partial u}{\partial y} + \frac{\partial u}{\partial t} \quad (A.4)$$

From the main text, the x-component of the expression in brackets is, for our specific c.v.:

$$R(\ddot{\alpha}\sin\phi + \dot{\alpha}^2\cos\phi) - 2\dot{\alpha}\dot{v} - \ddot{\alpha}y + \dot{\alpha}^2x$$

And therefore:

$$-\frac{1}{\rho}\frac{\partial P}{\partial x} - R(\ddot{\alpha}\sin\phi + \dot{\alpha}^2\cos\phi) - 2\dot{\alpha}\dot{v} - \ddot{\alpha}y + \dot{\alpha}^2x = \frac{u\partial u}{\partial x} + \frac{v\partial u}{\partial y} + \frac{\partial u}{\partial t} \quad (\text{A.5})$$

Applying (A.5) at the edge of the boundary layer and noting that $\partial U_e/\partial y = 0$, we get:

$$-\frac{1}{\rho}\frac{\partial P}{\partial x} = u_e \frac{\partial u_e}{\partial x} + \frac{\partial u_e}{\partial t} + R(\ddot{\alpha}\sin\phi + \dot{\alpha}^2\cos\phi) + 2\dot{\alpha}\dot{v}_e + \ddot{\alpha}\delta - \dot{\alpha}^2x \quad (\text{A.6})$$

(A.6) is the Euler equation applied at the edge of our particular non-inertial, unsteady control volume. As $\partial P/\partial x$ is by definition a function of x only, its value is the same across the height of the boundary layer for any given x . The value given by (A.6) can therefore be substituted in the momentum equation.

Appendix B

Unsteady Separation

For a steady boundary layer, separation occurs when the shear stress at the wall is zero; combining this with the no-slip condition, we see that the separation criteria is:

$$\begin{aligned} \text{at } y = 0 \quad U &= 0 \\ \partial u / \partial y &= 0 \end{aligned}$$

For a moving wall, however, the no-slip condition becomes

$$\text{at } y = 0 \quad U = U_{\text{WALL}}$$

In this case the Moore-Root-Sears (MRS) criterion for separation is that:

$$U = 0 \quad (\text{B.1a})$$

$$\partial u / \partial y = 0 \quad (\text{B.1b})$$

at some point in the interior of the boundary layer (8:427), as seen by an observer in the inertial reference frame. In this Appendix, we combined the RMS criterion with the momentum-integral method to find the value of Λ at separation for our pitching airfoil.

In our development of the von Karman-Pohlhausen method, we have assumed a velocity profile of the form:

$$\frac{u}{u_{\infty}} = A + B\eta + C\eta^2 + D\eta^3 + E\eta^4 \quad (\text{B.2})$$

and found that

$$A = 0 \quad (B.3a)$$

$$B = \frac{\Lambda + 12}{6} \quad (B.3b)$$

$$C = -\frac{\Lambda}{2} \quad (B.3c)$$

$$D = \frac{\Lambda - 4}{2} \quad (B.3d)$$

$$E = -\frac{\Lambda + 6}{6} \quad (B.3e)$$

Substituting (B.3) into (B.2), and applying (B.1b), we find that for separation to occur, the velocity profile must satisfy:

$$4\left(1 - \frac{\Lambda_s}{6}\right)\eta^3 + 3\left(\frac{\Lambda_s}{2} - 2\right)\eta^2 - \Lambda_s\eta + \left(2 + \frac{\Lambda_s}{6}\right) = 0 \quad (B.4)$$

where Λ_s is the value of the velocity profile shape parameter Λ at separation. The cubic polynomial (B.4) can be solved analytically (14:9). By applying the CRC method of solution, we find that (B.4) has three real roots:

$$\eta_1 = \frac{(\Lambda + 12)}{4(6 - \Lambda)} \quad (B.5a)$$

$$\eta_2 = \eta_3 = 1 \quad (B.5b)$$

These are then the value of η at which $\partial(U/U_\infty)/\partial\eta = 0$ or equivalently $\partial u/\partial y = 0$. The double root occurs at $\eta = 1$, i.e. at the edge of the boundary layer where $u = u_e$ and therefore $\partial u/\partial y = 0$ as normal. The first (B.5a) must then be the

solution for the moving wall separation. We note that it includes the steady wall solution because if we let η_1 be zero, we obtain $\Lambda_s = -12$ which is the steady wall separation criterion. Substituting (B.5a) back into (B.2), we get

$$\frac{u_s}{u_\infty} = \frac{(\Lambda_s + 12)^2}{512(\Lambda_s - 6)^3} (9\Lambda_s^2 - 136\Lambda_s + 528) \quad (B.6)$$

From the inertial reference $U = 0$ and again we recover $\Lambda = -12$ as the separation criterion. From the non-inertial reference frame, however, $U_s = -U_{WALL}$ or, for our pitching airfoil problem:

$$U_s = -\dot{\alpha} R \sin \phi \quad (B.7a)$$

$$U_\infty = U_e \quad (B.7b)$$

Combining (B.6) and (B.7), we get:

$$\frac{(\Lambda_s + 12)^2}{(\Lambda_s - 6)^3} (9\Lambda_s^2 - 136\Lambda_s + 528) = - \frac{512\dot{\alpha} R \sin \phi}{u_e} = DK \quad (B.8)$$

For given airfoil and test condition, (B.8) can be solved for Λ_s . Figure B.1 is a plot of the solution of equation (B.8) as a function of DK. When the value of Λ_s is reached at the quarter chord, separation is assumed to occur.

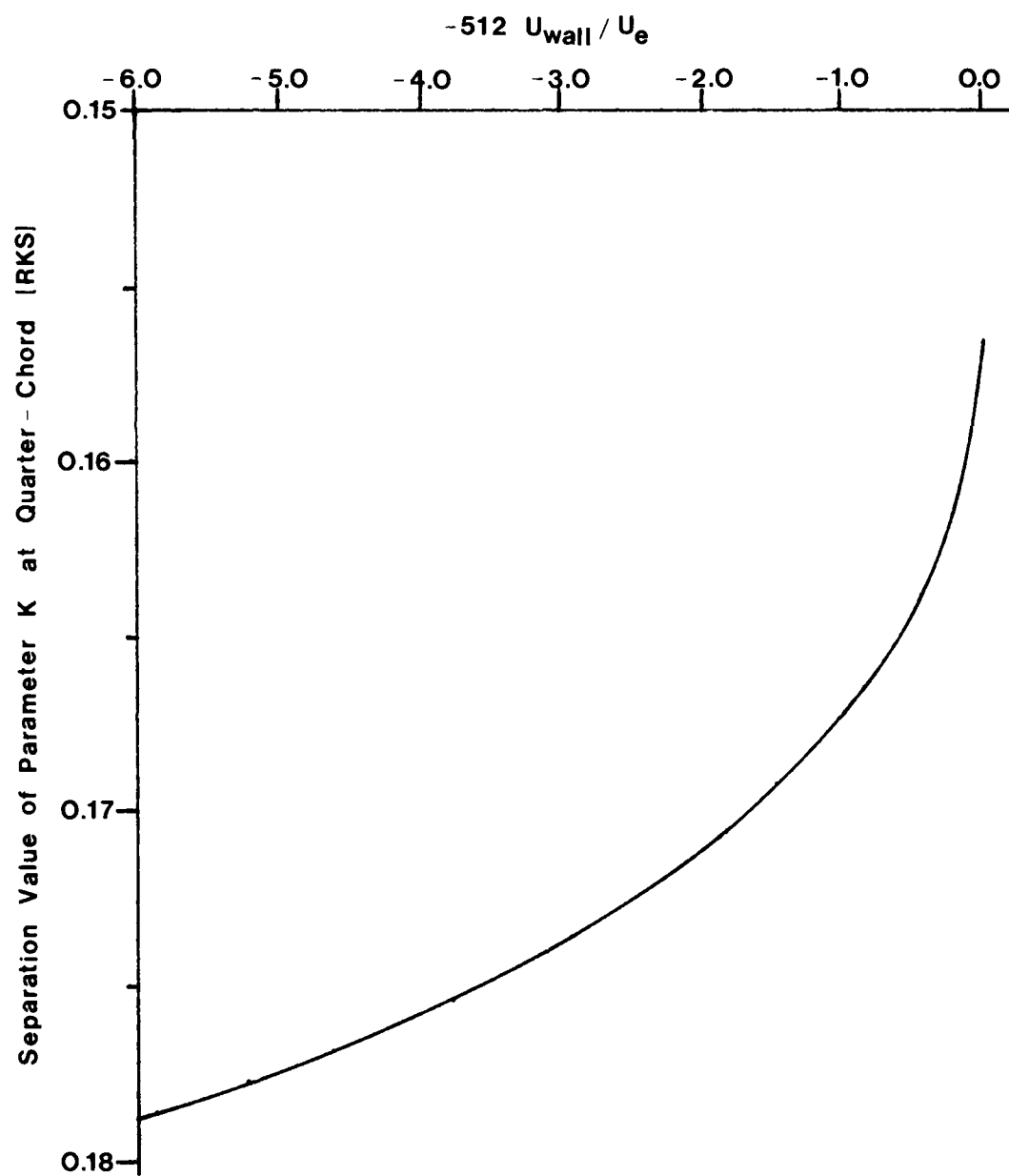


Figure B1. Unsteady Separation Criteria

```

*      Repeats program for next test conditions from FLOWIN2
*
      IF(ALPHA.LE.900)GO TO 125
1      FORMAT(4X,F6.3,2(4X,F10.3),4X,F7.3,4X,F7.4,4X,F8.4,2(4X,E9.3))
12     FORMAT(////////)
30     FORMAT(1H1,"BOUNDARY-LAYER PARAMETERS FOR ",F6.2,"FT/SEC"/)
40     FORMAT(" INITIAL ANGLE OF ATTACK: ",F6.3," DEGREES"/)
45     FORMAT("/ FINAL ANGLE OF ATTACK: ",F6.3," DEGREES"/)
50     FORMAT(" PITCH RATE: ",F7.3," DEGREES/SEC"/)
52     FORMAT(6X,"XOC",10X,"U",11X,"DUDS",9X,"DUDT",8X,"FK",
+      9X,"RK",11X,"Z",11X,"DZDS"/)
55     FORMAT(" PITCH PARAMETER: ",F7.5/)
60     FORMAT(" K AT THE QUARTER-CHORD: ",F8.4/)
66     FORMAT(" STALLING COEFF (DK): ",F8.4/)
65     FORMAT("chord= ",F8.4,10X,"angle for 0.25c ",F8.4////)
80     FORMAT(" TIME TO REACH THE QUARTER-")
81     FORMAT(" CHORD FROM THE STAGNATION POINT: ",F7.5," SEC"/)
85     FORMAT(" UWALL/UE AT THE QUARTER-CHORD: ",E9.3/)
89     FORMAT("airfoil geometry amu= ",f6.3,3x,"bmu= ",f6.3/)
88     FORMAT("rotation point in fraction of chord (+ after 0.5c",
+      "- before): ",f9.3/)
*
      STOP
100    END
*
*
      SUBROUTINE U(ANGLE,RADIUS,CON,EI,UINF,AMU,BMU,ALPHA,UU)
      COMPLEX CMPLX,Z,EI,DZETA,W
*
*      Function of this subroutine is to to compute the local
*      value of velocity on a Joukowski airfoil using complex
*      potential flow theory.
*
      ANGLA=ANGLE-ALPHA
      X=RADIUS*COS(ANGLA*CON)
      Y=RADIUS*SIN(ANGLA*CON)
      Z=CMPLX(X,Y)
      W=UINF*((1.,0.)-(RADIUS**2)/Z**2+
+      (2.*EI*RADIUS*SIN(ALPHA*CON))/Z)
      X=X+AMU
      Y=Y+BMU
*
*      Z changed to represent values of coordinates used in
*      the transformation equation.
*
      Z=CMPLX(X,Y)
      DZETA=(Z**2-1.)/Z**2
      UU=CABS(W)/CABS(DZETA)
      RETURN
      END
*

```

```

CALL U(ANGLE,RADIUS,CON,EI,UINF,AMU,BMU,ALPH1,U2C)
CALL NIU(ANGLE,RADIUS,CON,AMU,BMU,ADOT2,X1,Y1,XROT
+ ,U2C,U2,RAS2,RAC2,DK)

```

```

*
*   Compute the unsteady velocity gradient.
*

```

```

DUDT=(U2-U1)/DELT
ANGLE=ANGLE-0.01
ANGLE1=ANGLE-0.01
CALL U(ANGLE1,RADIUS,CON,EI,UINF,AMU,BMU,ALPH1,U2C)
CALL DS(ANGLE1,RADIUS,CON,AMU,BMU,X2,Y2)
CALL NIU(ANGLE1,RADIUS,CON,AMU,BMU,ADOT2,X2,Y2,XROT
+ ,U2C,U2,RAS2,RAC2,DK)
ANGLE0=ANGLE+0.01
CALL U(ANGLE0,RADIUS,CON,EI,UINF,AMU,BMU,ALPH1,U0C)
CALL DS(ANGLE0,RADIUS,CON,AMU,BMU,X0,Y0)
CALL NIU(ANGLE0,RADIUS,CON,AMU,BMU,ADOT2,X0,Y0,XROT
+ ,U0C,U0,RAS0,RAC0,DK)
CALL U(ANGLE,RADIUS,CON,EI,UINF,AMU,BMU,ALPH1,U1C)
CALL DS(ANGLE,RADIUS,CON,AMU,BMU,X1,Y1)
CALL NIU(ANGLE,RADIUS,CON,AMU,BMU,ADOT2,X1,Y1,XROT
+ ,U1C,U1,RAS1,RAC1,DK)

```

```

*
*   Compute arc length and velocity gradient.
*

```

```

DS1=(SQRT((X1-X0)**2+(Y1-Y0)**2))/CHORD
DS2=(SQRT((X2-X1)**2+(Y2-Y1)**2))/CHORD
DSS=DS1+DS2
DUDS=(U2-U0)/DSS
UDUDS=U1*DUDS
XOC=(X1+XLE)/CHORD

```

```

*
*   Stop the computation at the quarter-chord, but only when
*   it is reached on the upper surface.
*

```

```

IF((XOC.GE.0.250).AND.(XOC.GT.OLDXOC)) GO TO 25
OLDXOC=XOC
IF(N.LT.250) GO TO 20
N=0

```

```

20  WRITE(16,1)XOC,U1,DUDS,DUDT,FK,RK,ZZ,DZDS
    CONTINUE

```

```

*
25  WRITE(16,1)XOC,U1,DUDS,DUDT,FK,RK,ZZ,DZDS
    WRITE(16,45)ALPH1
    WRITE(16,55)PITCH
    WRITE(16,60)RK
    WRITE(16,80)
    WRITE(16,81)TIME
    UMIN=RAS1/U1
    WRITE(16,85)UMIN

```



```

DS1=(SQRT((X1-X0)**2+(Y1-Y0)**2))/CHORD
DS2=(SQRT((X2-X1)**2+(Y2-Y1)**2))/CHORD

```

```

*
* Compute the arc length and the velocity gradient.
*

```

```

DSS=DS1+DS2
DUDS=(U2-U0)/DSS
XOC=(X1+XLE)/CHORD
IF(N.LT.50) GO TO 10
N=0
WRITE(16,1)XOC,U1,DUDS,DUDT,FK,RK,ZZ,DZDS
10 CONTINUE

```

```

*
* ADOT=ADOT1
* N=0
* RAS1=0.0
* RAC1=0.0
* DO 20 J=K1,K2

```

```

*
* Function of this loop is to compute the behavior
* of the boundary layer as it is subjected to a
* pitching motion.
*

```

```

N=N+1

```

```

*
* Compute the pertinent boundary layer parameters.
*

```

```

ZZ=DZDS*DS1+ZZ
RK=ZZ*(DUDS*(1.+RAS1/U1)+DUDT/U1)
CALL POHL(RK,RLAMDA)
DEL2=37./315.-RLAMDA/945.-(RLAMDA**2)/9072.
FK=2.*DEL2*(2.-.3683*RLAMDA+.0104*RLAMDA**2+
+ (RLAMDA**3)/4536.)
F1K=(.3-RLAMDA/120.)/DEL2
RMIC=4.0

```

```

*
* RMIC is the mass injection constant.
*

```

```

DZDS=(FK+(4.+F1K)*ZZ*DUDT/U1+(4.+2.*FF1K-2./DEL2)*ZZ
+ *RAS1*DUDS/U1-2.*RMIC*ZZ*RAC1/DEL2)/U1

```

```

*
* Compute the time increment for a particle to
* travel from point (i) to point (i+1).
*

```

```

DELT=CHORD*DS1/U1
TIME=TIME+DELT
DALPHA=DELT*ADOT
ANGLE=ANGLE+DALPHA
ALPH1=ALPH1+DALPHA

```

```

*      DUDS=(U2-U0)/(DS1+DS2)
*
*      Second derivative of velocity computed using a
*      Taylor's series expansion.
*
*      D2UDS2=(U2-2.*U1+U0)/((DS1+DS2)/2.)*2
*
*      Enter initial boundary layer parameters.
*
*      RLAMDA=7.052
*      RK=0.0770
*      FK=0.0
*      DZDS=-0.0652*D2UDS2/(DUDS**2)
*      ZZ=RK/DUDS
*
*      N=50
*      ANGLE=2*ALPHA+THETA-0.01
*      XOC=(X0+XLE)/CHORD
*      WRITE(16,1)XOC,U0,DUDS,D2UDS2,FK,RK,ZZ,DZDS
*
*      ADOT=0.0
*      DO 10 J=1,K
*
*      Function of this loop is to compute boundary layer
*      parameters at stagnation point, allowing the
*      boundary layer to steady-out before subjecting it
*      to a pitching motion.
*
*      N=N+1
*
*      Compute pertinent boundary layer parameters.
*
*      ZZ=DZDS*DS1+ZZ
*      RK=ZZ*DUDS
*      FK=.47-6.*RK
*      DZDS=FK/U1
*
*      DELT=CHORD*DS1/U1
*      TIME=TIME+DELT
*      CALL U(ANGLE,RADIUS,CON,EI,UINF,AMU,BMU,ALPHA,U2)
*      DUDT=(U2-U1)/DELT
*      ANGLE=ANGLE-0.01
*      ANGLE1=ANGLE-0.01
*      CALL U(ANGLE1,RADIUS,CON,EI,UINF,AMU,BMU,ALPHA,U2)
*      CALL DS(ANGLE1,RADIUS,CON,AMU,BMU,X2,Y2)
*      ANGLE0=ANGLE+0.01
*      CALL U(ANGLE0,RADIUS,CON,EI,UINF,AMU,BMU,ALPHA,U0)
*      CALL DS(ANGLE0,RADIUS,CON,AMU,BMU,X0,Y0)
*      CALL U(ANGLE,RADIUS,CON,EI,UINF,AMU,BMU,ALPHA,U1)
*      CALL DS(ANGLE,RADIUS,CON,AMU,BMU,X1,Y1)

```

```

*
XP=90.
XN=180.
7  XM=(XP+XN)/2.
    CALL DS(XM,RADIUS,CON,AMU,BMU,XC,YC)
    IF(ABS(XP-XN).LT.0.00001) GO TO 11
    FFXM=((XC+XLE)/CHORD)-0.250
        IF(FXM.LT.0.0) GO TO 8
        IF(FXM.EQ.0.0) GO TO 11
        IF(FXM.GT.0.0) GO TO 9
8   XN=XM
    GO TO 7
9   XP=XM
    GO TO 7
1  CONTINUE
    ANGLQC=XM
    CALL U(ANGLQC,RADIUS,CON,EI,UINF,AMU,BMU,ALPHA,UC)
    CALL NIU(ANGLQC,RADIUS,CON,AMU,BMU,ADOT2,XC,YC,XROT,UC,
+   UNI,RAS2,RAC2,DK)
    DK=-512.*ADOT2*DK
    PITCH=ADOT1*CON*0.5*CHORD/UINF
*
K=100
K1=K+1
K2=(ALPHA+150)*100+K
*
WRITE(16,12)
WRITE(16,30)UINF
WRITE(16,40)ALPHA
WRITE(16,50)ADOT1
WRITE(16,89)AMU,BMU
WRITE(16,88)XROT
WRITE(16,65)CHORD,ANGLQC
WRITE(16,66)DK
WRITE(16,52)
*
ANGLE=2*ALPHA+THETA
CALL U(ANGLE,RADIUS,CON,EI,UINF,AMU,BMU,ALPHA,U0)
CALL DS(ANGLE,RADIUS,CON,AMU,BMU,X0,Y0)
ANGLE=ANGLE-0.01
CALL U(ANGLE,RADIUS,CON,EI,UINF,AMU,BMU,ALPHA,U1)
CALL DS(ANGLE,RADIUS,CON,AMU,BMU,X1,Y1)
ANGLE=ANGLE-0.01
CALL U(ANGLE,RADIUS,CON,EI,UINF,AMU,BMU,ALPHA,U2)
CALL DS(ANGLE,RADIUS,CON,AMU,BMU,X2,Y2)
DS2=(SQRT((X2-X1)**2+(Y2-Y1)**2))/CHORD
DS1=(SQRT((X1-X0)**2+(Y1-Y0)**2))/CHORD
*
*   Stagnation point velocity gradient computed using a
*   forward difference method; all other velocity gradients
*   computed using central difference method.

```

```

*      BETA = local slope of airfoil surface.
*      RAS1,RAC1 = functions (of geometry) due to pitching motion.
*      RLAMDA,RK = Pohlhausen shape parameters.
*      FK,ZZ,DZDS,DEL2,F1K = functions of shape parameters.
*      XROT = Location of the rotation in percent chord, with
*             respect to the mid-chord position. A negative is
*             interpreted as forward of the mid-chord position.
*      TH1 = Angle on the circle mapping to the trailing edge
*      TH2 = Angle on the circle mapping to the leading edge
*      DK = The quarter-chord separation parameter accounting
*           for the MRS separation condition of a moving wall
*      RMIC = The mass ingestion constant

```

```

PROGRAM POHL10
COMPLEX EI
OPEN (15,FILE='FLOWIN2')
REWIND 15
OPEN (16,FILE='FLOWOUT2')
REWIND 16
EI=(0.,1.)
125 READ (15,*,END=100) ALPHA,ADOT1,UINF,AMU,BMU,XROT
RADIUS=SQRT((1.-AMU)**2+BMU**2)
OLDXOC=1.
ALPH1=ALPHA
CON=3.1415927/180.
ADOT2=ADOT1*CON
TH1=-(ATAN(BMU/(1.-AMU)))/CON
TH2=180.-TH1
THETA=180.
TIME=0.0

```

```

*
*      Compute chord length
*
CALL DS(TH2,RADIUS,CON,AMU,BMU,XLE,YLE)
CALL DS(TH1,RADIUS,CON,AMU,BMU,XTE,YTE)
C=SQRT((YLE-YTE)**2+(XLE+XTE)**2)
CHORD=C
4  TH2=TH2+0.02
CALL DS(TH2,RADIUS,CON,AMU,BMU,XC,YC)
C=SQRT((YTE-YC)**2+(XTE-XC)**2)
IF(C.GT.CHORD) THEN
    CHORD=C
    GO TO 4
ELSE
    GO TO 6
END IF
6  ANGLE=TH2-0.01
CALL DS(ANGLE,RADIUS,CON,AMU,BMU,XLE,YLE)
XLE=ABS(XLE)

```

```

*
*      Find the angle mapping to 0.25c

```

Appendix D

Computer Program POHL KP 84S

POHL KP 84S: pitching airfoil with mass introduction.

NOTE :mass ingestion may be turned off by assingning
0.0 to the mass ingestion constant RMIC, on line 235

ALLAIRE, Andre J.S.
GAE-84S

This program is adapted from program "POHL2", Docken,
GAE-82D, and "POHL6", Lawrence, GAE-83D. It will be used
to continue analysis work in the area of dynamic stall
effects. The representative airfoil is a 15% Joukowski
pitching at a constant rate about its mid-chord in a
steady freestream; however, any thickness or camber
ratio, as well as location of rotation point, may be
specified. If desired, mass may be injected into the
boundary layer from the freestream to model the non-
Newtonian motion of the airfoil.

Symbology used within this program is as follows:

EI = imaginary unit; i.e., square root of -1.
RADIUS = radius of circular cylinder.
AMU,BMU=offset distance of center of circular cylinder.
ALPHA = angle of attack, in degrees.
ADOT1 = pitch rate, in degrees per second.
PITCH = non-dimensional pitch rate.
CHORD = chord-length of Joukowski airfoil.
ANGLE = radial of a given point on the circular cylinder.
UINF = freestream velocity, in feet per second.
CON = conversion factor, degrees to radians.
X,Y,U = coordinates and potential flow velocity on airfoil.
Z,W = complex coordinates and velocity.
UMIN = ratio of wall velocity to potential flow velocity.
TIME = cumulative time.
DELT = increment of time.
K,N = integer counters.
DSS = increment of distance on the airfoil surface.
DUDS = spatial partial derivative of velocity.
DUDT = partial derivative of velocity wrt time.
XOC = chord position.

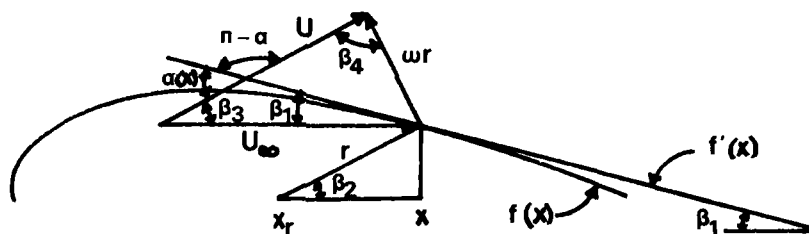
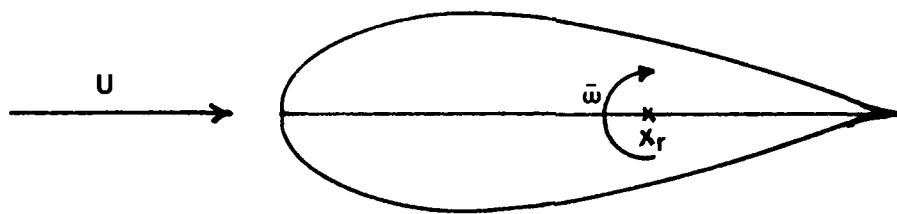


Figure C4. Thick Airfoil

to consider separately the upper and lower surface. From Figure C4, we see that for the upper surface:

$$\alpha = \beta_1 + \beta_3 \quad (C.12)$$

$$r = \sqrt{f^2(x) + (x - x_r)^2} \quad (C.13)$$

$$\tan \beta_1 = f'(x) \quad (C.14)$$

$$\tan \beta_2 = \frac{f(x)}{(x - x_r)} \quad (C.15)$$

$$\beta_4 = \frac{\pi}{2} + \beta_2 - \beta_3 \quad (C.16)$$

and from the law of sines:

$$\frac{U_\infty}{\sin \beta_4} = \frac{\omega r}{\sin \beta_3} \quad (C.17)$$

for six equations in six unknowns. Unfortunately, the system is transcendental and cannot be solved analytically. However, one can see from the figure C4, that the head of the vector ωr is shifted to the left as a result of thickness, and we get a higher local angle of attack than for the flat plate, which results therefore in the creation of more induced camber. This additional camber could explain the higher ΔC_l predicted by Tupper for the J015 airfoil.

Jumper (15) has shown that for the case of a parabolic camber distribution, the zero lift angle of attack is

$$\alpha_{\ell 0} = -2Z_c/c \quad (C.8)$$

where Z_c/c is the camber ratio. Using this, our pitching plate has:

$$\alpha_{\ell 0} = -\dot{\alpha}_{ND}/2 \quad (C.9)$$

For a thin flat plate at small angle of attack, the theoretical lift coefficient is (16:2-8)

$$C_\ell = 2\pi\alpha \quad (C.10)$$

The rotation has therefore induced an increase in lift coefficient of:

$$\Delta C_\ell = \pi \dot{\alpha}_{ND} \quad (C.11)$$

In his trailing edge vortex method, Tupper found, "empirically," that for a flat plate $\Delta c_\ell = 3.14 \dot{\alpha}_{ND}$ our analytical solution confirms his result with remarkable accuracy. Furthermore, for a Joukowski J015 airfoil, Tupper found (6:42) a jump in c_ℓ of $3.47 \dot{\alpha}_{ND}$. Without solving the solution analytically, the next section provides an argument showing thickness may increase the value of the induced camber.

Thick Airfoil

The same procedure can be repeated for the case of a general thick and cambered airfoil. In this case, we need

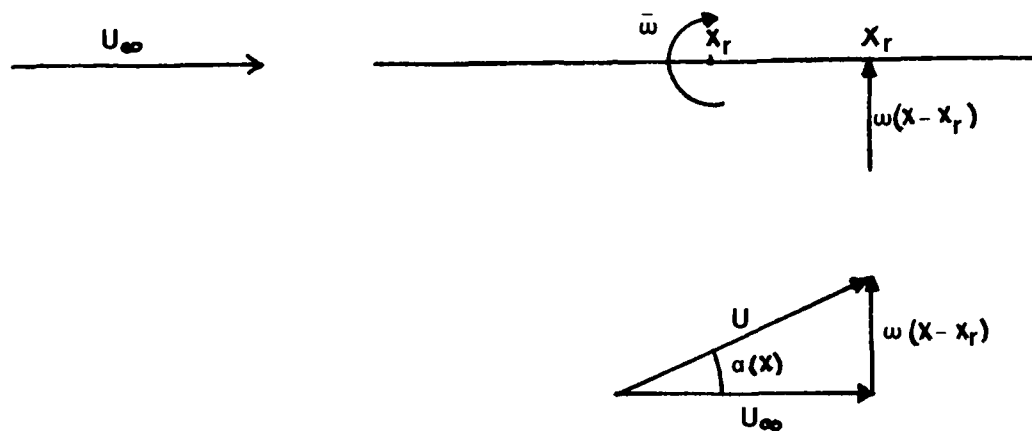


Figure C2. Local Angle of Attack on Rotating Flat Plate

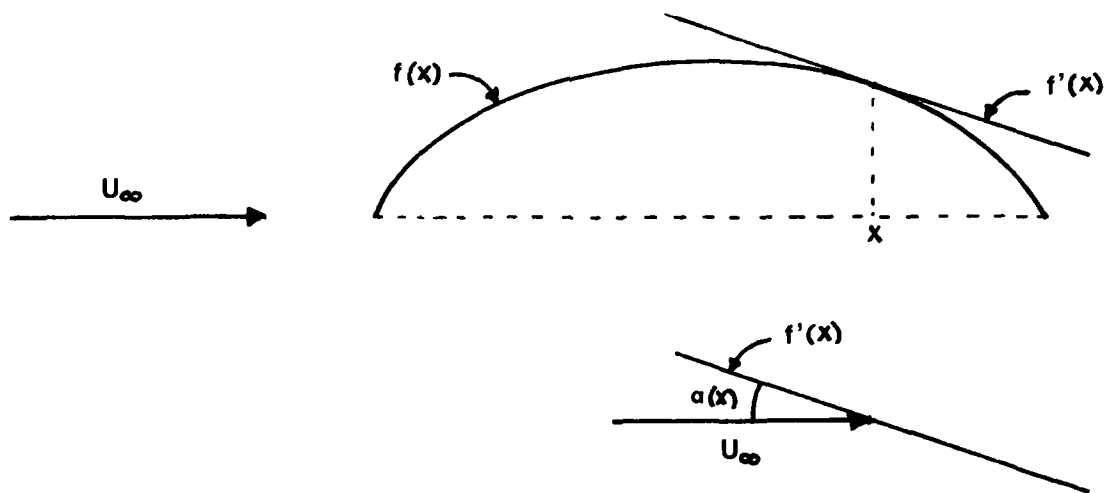


Figure C3. Local Angle of Attack on Cambered Plate

To find the equation of the equivalent cambered plate, we simply need to solve the differential equation (C.3). As ω , x_r and U are not a function of x , the solution of equation (C.3) is:

$$f(x) = -\frac{\omega}{2U_\infty} x^2 + \frac{x_r \omega}{U_\infty} x + k$$

The integration constant k , is evaluated by imposing $f(x) = 0$ at $x = x_{LE} = 0$ (leading edge). Then $k = 0$ and

$$f(x) = -\frac{\omega}{2U_\infty} (x^2 - 2x_r x) \quad (C.4)$$

If we non-dimensionalize with respect to the chord:

$$f(x/c) = -\dot{\alpha}_{ND} \frac{x^2}{c^2} - \frac{2x_r x}{c^2}$$

where

$$\dot{\alpha}_{ND} = \frac{\omega c}{2U_\infty} \quad (C.5)$$

This equation shows that the induced camber is parabolic. By equating the first derivative of (C.5) to zero, we find that the maximum of the camber function occurs for $(x/c) = (x_r/c)$, i.e. at the rotation point. There,

$$f(x_r/c) = \dot{\alpha}(x_r/c)^2 \quad (C.6)$$

Finally, we note that

$$f(1) = 2(x_r/c) - 1 \quad (C.7)$$

For the special case where $x_r = 0.5c$, $f(1) = 0$ and the induced camber ratio is $\dot{\alpha}_{ND}/4$.

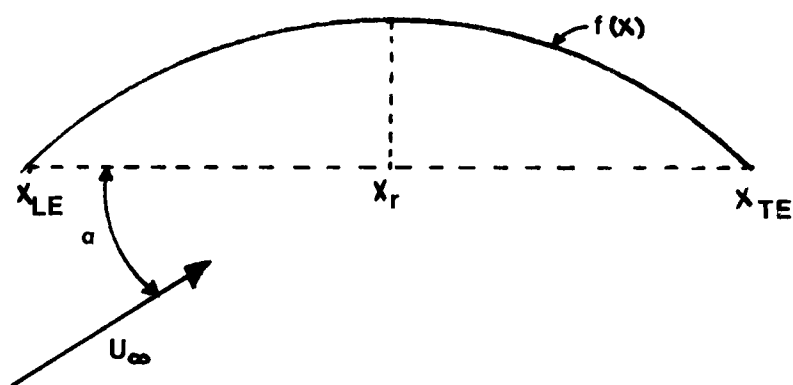
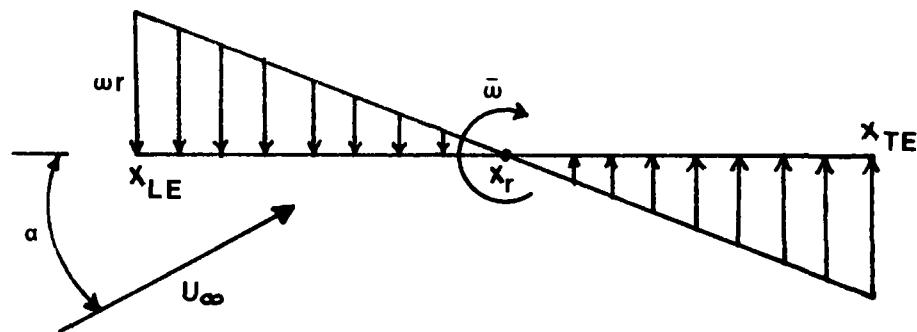


Figure C1. Induced Camber on a Flat Plate

Appendix C

Camber Induced by Rotation

When an airfoil rotates in a steady flow, the local angle of attack changes along the surface of the airfoil, as can be inferred from the pitching flat plate of figure C1. It is then possible to model a pitching airfoil by a non-pitching one having some camber induced by the pitching motion. The amount of camber equivalent to a given pitching rate is computed in this Appendix. We consider first the simple case of a flat plate instantaneously at zero angle of attack before generalizing to a thick airfoil.

Pitching Flat Plate

From figure C2, we see that the local angle of attack seen by a pitching flat plate, for a general point x on the plate, is given by:

$$\tan \alpha(x) = \frac{\omega(x - x_r)}{U_\infty} \quad (C.1)$$

In the case of a non-pitching but cambered plate, if $f(x)$ represents the locus of points of the camber in the same flow, its local angle of attack is given by:

$$\tan \alpha(x) = -f'(x) \quad (C.2)$$

Equating (C.1) and (C.2) gives:

$$f'(x) = - \frac{\omega(x - x_r)}{U_\infty} \quad (C.3)$$

```

*
SUBROUTINE DS(ANGLE,RADIUS,CON,AMU,BMU,X,Y)
COMPLEX CMPLX,Z
*
* Function of this subroutine is to compute the pos-
* ition of a point on the airfoil, given its position
* on the mapping circle.
*
X=RADIUS*COS(ANGLE*CON)+AMU
Y=RADIUS*SIN(ANGLE*CON)+BMU
Z=CMPLX(X,Y)
Z=Z+1./Z
X=REAL(Z)
Y=AIMAG(Z)
RETURN
END
*
*
SUBROUTINE POHL(RK,RLAMDA)
*
* Function of this subroutine is to compute the value
* of the separation parameter, lamda, giiven a value
* of K, as computed in the main program.
*
RK1=-.160
RK2=-.112
RK3=0.00
RK4=0.06
RK5=0.076
RK6=0.086
RK7=0.0949
IF(RK.LE.RK1) GO TO 10
IF(RK.LE.RK2) GO TO 20
IF(RK.LE.RK3) GO TO 30
IF(RK.LE.RK4) GO TO 40
IF(RK.LE.RK5) GO TO 50
IF(RK.LE.RK6) GO TO 60
IF(RK.GT.RK7) GO TO 70
*
RLAMDA=.0149**2-(RK-0.08)**2
RLAMDA=12.-100.*SQRT(RLAMDA)
RETURN
*
10  RLAMDA=(2./0.012)*RK+14.0
RETURN
*
20  RLAMDA=(4./0.044)*RK+2.18
RETURN
*
30  RLAMDA=(10./0.14)*RK
RETURN

```

```

*      40      RLAMDA=83.33*RK
*             RETURN
*
*      50      RLAMDA=-1.9+115.*RK
*             RETURN
*
*      60      RLAMDA=-6.54+176.*RK
*             RETURN
*
*      70      RLAMDA=12.
*             RETURN
*             END
*
*
*      SUBROUTINE NIU(ANGLEC,RADIUS,CON,AMU,BMU,ADOT2,XC,YC,
+      XROT,UC,UNI,RASF,RACF,DK)
*
*      Function of this subroutine is to compute the value of U in
*      the non-inertial reference frame, and the values of the
*      required functions of geometry, as a function of the airfoil
*      shape and the location of the rotation point. The value of
*      the quarter-chord separation parameter DK is also computed
*      this subroutine.
*
*      R=SQRT(XC**2+YC**2)
*      BET1=ATAN(YC/(-XC))
*      ANGLEM=ANGLEC+.1
*      ANGLEP=ANGLEC-.1
*      CALL DS(ANGLEM,RADIUS,CON,AMU,BMU,XM,YM)
*      CALL DS(ANGLEP,RADIUS,CON,AMU,BMU,XP,YP)
*      DY=ABS(YP-YM)
*      DX=ABS(XP-XM)
*      Q=1000.*DX
*      IF(DY.GT.Q)THEN
*      BETA=1.5707963
*      ELSE
*      BETA=BET1+ATAN(DY/DX)
*      END IF
*      RP=SQRT(YC**2+(XROT-XC)**2)
*      ANG=ABS((RP**2+R**2-XROT**2)/(2.*R*RP))
*      IF(ANG.GE.1.0 ) THEN
*      DELTA1=0.0
*      ELSE
*      DELTA1=ACOS(ANG)
*      END IF
*      R=RP
*      IF(XROT.GE.0.0)THEN
*      BETA=BETA-DELTA1
*      ELSE
*      BETA=BETA+DELTA1

```

```
END IF  
RAS $F$ = $R$ * $\dot{A}$ * $\sin(\beta)$   
RAC $F$ = $R$ * $\dot{A}$ * $\cos(\beta)$   
UNI= $U$ -RAS $F$   
DK= $R$ * $\sin(\beta)$ /UNI  
RETURN  
END
```

VITA

Major André J.S. Allaire was born on 22 April 1948 in Trois-Rivières, Québec, Canada. He graduated from high school in Trois-Rivières in 1967 and attended the Collège Militaire royal de St-Jean, from which he received the degree of Bachelor of Science in Mathematics and Physics in May 1972. Upon graduation, he was commissioned a Lieutenant in the Canadian Armed Forces (CAF). He served in several managerial and engineering positions with the CAF. He obtained a license in Business Administration from McGill University, Montreal in 1977. He graduated from the "Ecole du Personal Naviguant d'Essai et de Réception" (EPNER), Ystres, France as a Flight Test Engineer in 1979 and worked in different Flight Test programs at the Aerospace Engineering and Testing Establishment (AETE) in CFB Cold Lake, Alberta, Canada, until entering the School of Engineering, Air Force Institute of Technology, in August 1982.

Permanent Address: 8 Monté-Carlo
Gatineau, Québec
Canada
J8T 5K6

UNCLASSIFIED

SECURITY CLASSIFICATION OF THIS PAGE

REPORT DOCUMENTATION PAGE

1a. REPORT SECURITY CLASSIFICATION UNCLASSIFIED			1b. RESTRICTIVE MARKINGS	
2a. SECURITY CLASSIFICATION AUTHORITY			3. DISTRIBUTION/AVAILABILITY OF REPORT Approved for public release distribution unlimited.	
2b. DECLASSIFICATION/DOWNGRADING SCHEDULE				
4. PERFORMING ORGANIZATION REPORT NUMBER(S) AFIT/GAE/AA/84S-1			5. MONITORING ORGANIZATION REPORT NUMBER(S)	
6a. NAME OF PERFORMING ORGANIZATION School of Engineering		6b. OFFICE SYMBOL (If applicable) AFIT/EN		7a. NAME OF MONITORING ORGANIZATION
6c. ADDRESS (City, State and ZIP Code) Air Force Institute of Technology Wright-Patterson AFB, Ohio 45433			7b. ADDRESS (City, State and ZIP Code)	
8a. NAME OF FUNDING/SPONSORING ORGANIZATION		8b. OFFICE SYMBOL (If applicable)		9. PROCUREMENT INSTRUMENT IDENTIFICATION NUMBER
8c. ADDRESS (City, State and ZIP Code)			10. SOURCE OF FUNDING NOS.	
			PROGRAM ELEMENT NO.	PROJECT NO.
			TASK NO.	WORK UNIT NO.
11. TITLE (Include Security Classification) See Box 19				
12. PERSONAL AUTHOR(S) Andre J.S. Allaire, B.S., Major, CAF				
13a. TYPE OF REPORT MS Thesis		13b. TIME COVERED FROM _____ TO _____		14. DATE OF REPORT (Yr., Mo., Day) 1984 September
15. PAGE COUNT 85				
16. SUPPLEMENTARY NOTATION				
17. COSATI CODES			18. SUBJECT TERMS (Continue on reverse if necessary and identify by block number)	
FIELD	GROUP	SUB. GR.	Dynamic Stall, Pitching Airfoil; Boundary Layer, Unsteady Momentum-Integral Method; MRS Model; Mass Introduction; Induced Camber.	
19. ABSTRACT (Continue on reverse if necessary and identify by block number)				
Title: INVESTIGATION OF POTENTIAL AND VISCOUS FLOW EFFECTS CONTRIBUTING TO DYNAMIC STALL				
Thesis Chairman: Eric J. Jumper, Major, USAF				
Approved for public release, IAW AFR 190-17. LYNN E. WOLAVER 231453 Dean for Research and Professional Development Air Force Institute of Technology (AIC) Wright-Patterson AFB OH 45422				
20. DISTRIBUTION/AVAILABILITY OF ABSTRACT UNCLASSIFIED/UNLIMITED <input checked="" type="checkbox"/> SAME AS RPT. <input type="checkbox"/> DTIC USERS <input type="checkbox"/>			21. ABSTRACT SECURITY CLASSIFICATION UNCLASSIFIED	
22a. NAME OF RESPONSIBLE INDIVIDUAL Eric J. Jumper, Major, USAF			22b. TELEPHONE NUMBER (Include Area Code) 513-255-3517	22c. OFFICE SYMBOL AFIT/ENY

Abstract

This study explores the problem of dynamic stall, i.e. the stall of an airfoil undergoing pitching motion. The general equations of continuity and momentum are developed for a non-inertial and unsteady control volume. They are written in momentum-integral form and the boundary layer on the pitching airfoil is computed using a modified von Karman-Pohlhausen method.

The boundary layer edge velocity, velocity gradient and time rate of change of velocities required for the step by step integration of the von Karman-Pohlhausen working equations are obtained from the inviscid solution. The inviscid velocity profile along the surface of the airfoil is obtained by conformal mapping from the velocity profile around a rotating circular cylinder. Complex potential flow theory is used to obtain the velocity around the cylinder. The Kutta condition is continuously maintained at the point mapping to the trailing edge of the airfoil for each time step. This way, the flow is considered steady at each time step, but varies from one time step to the next when the angle of attack is increased. The increase in stall angle of attack is analyzed as a function of a non-dimensional pitch rate, $(0.5c\dot{\alpha}/U_\infty)$. Although the solution is obtained primarily for a symmetric Joukowski airfoil of thickness ratio 0.15 (J015), the analysis also includes variations of camber, thickness and location of the point of rotation.

END

FILMED

5-85

DTIC